

Soft Robotics

Journal Name: <http://mc.manuscriptcentral.com/master0>

Twisted-and-Coiled Actuators with Free Strokes Enable Soft Robots with Programmable Motions

Journal:	<i>Soft Robotics</i>
Manuscript ID:	SORO-2019-0175.R1
Manuscript Type:	Original Article
Date Submitted by the Author:	n/a
Complete List of Authors:	Sun, Jiefeng; Colorado State University, Department of Mechanical Engineering Tighe, Brandon; Colorado State University, Department of Mechanical Engineering Liu, Yingxiang; Harbin Institute of Technology, State Key Laboratory of Robotics and System Zhao, Jianguo; Colorado State University, Department of Mechanical Engineering
Keyword:	soft manipulation < Robotics Field, Artificial muscles < Electronics and Materials Field, Highly deformable robots < Robotics Field
Manuscript Keywords (Search Terms):	Twisted-and-Coiled Actuator, Free Stroke, Programable Motion, Soft Robots
Note: The following files were submitted by the author for peer review, but cannot be converted to PDF. You must view these files (e.g. movies) online.	
SunVideoS1.mp4 SunVideoS2.mp4 SunVideoS3.mp4 SunVideoS4.mp4 SunVideoS5.mp4 SunVideoS6.mp4 SupplementaryMaterialSourceFile_Sun.zip	

SCHOLARONE™
Manuscripts

Twisted-and-Coiled Actuators with Free Strokes Enable Soft Robots with Programmable Motions

Jiefeng Sun¹, Brandon Tighe¹, Yingxiang Liu², and Jianguo Zhao¹

¹ Jiefeng Sun, Brandon Tighe, and Jianguo Zhao are with the Department of Mechanical Engineering at Colorado State University, Fort Collins, CO, 80523, USA.

² Yingxiang Liu is with the State Key Laboratory of Robotics and System, Harbin Institute of Technology, Harbin, 150001, China.

To whom correspondence should be addressed: jianguo.zhao@colostate.edu

Abstract

Various actuators (e.g., pneumatics, cables, dielectric elastomers, etc.) have been utilized to actuate soft robots. Besides widely used actuators, a relatively new artificial muscle — twisted-and-coiled actuators (TCAs) — is promising for actuating centimeter-scale soft robots because they are low-cost, have a large work density, and can be driven by electricity. However, existing works on TCA-actuated soft robots in general can only generate simple bending motion. The reason is that TCAs fabricated with conventional methods have to be preloaded to generate a large contraction, and thus cannot actuate soft robots properly. In this work, [an upgraded](#) technique is presented to fabricate TCAs that can deliver 48% free strokes (contraction without preloading). We first compare the static performance of TCAs with free strokes to conventional TCAs, and then characterize how will the fabrication parameters influence the TCAs' stroke and force capability. After that, we demonstrate that such TCAs can actuate centimeter-scale soft robots with programmable motions (gripping, twisting, and three-dimensional bending). Finally, we combine those motions to demonstrate a soft robotic arm that can perform a pick-and-place task. We expect TCAs with free strokes can enable miniature soft robots with rich three-dimensional motions for both locomotion and manipulation. Because TCAs are electrical driven, we can also potentially develop untethered soft robots by carrying onboard batteries and control circuits.

1 **1 Introduction**

2
3
4
5
6
7
8 Inspired by biological systems (e.g., octopus), soft robots made from soft materials
9 outperform traditional rigid robots in terms of safety and adaptivity owing to their compliant and
10 deformable bodies¹. To enable their unique capabilities, soft robots require a key component – the
11 actuator. Many different actuators have been used, including the conventional pneumatic-driven²
12 and cable-driven methods³, as well as several novel approaches proposed recently such as
13 combustion⁴, dielectric elastomers⁵ with variations⁶, chemical reactions⁷, liquid-vapor
14 transition⁸, liquid crystal elastomer⁹, and shape memory alloy^{10,11}.

15
16
17
18
19
20 Besides existing actuation approaches, another promising actuator for soft robots is the
21 twisted-and-coiled actuator (TCA), which can be conveniently fabricated by continuously twisting
22 polymer fibers into coiled spring-like shape¹². Compared with existing actuation methods, TCAs
23 exhibit several unique characteristics: 1) they are low cost since the polymer fibers used to
24 fabricate them can be commonly used household fibers (e.g., sewing threads or fishing line); 2)
25 they have a large work density (27.1 kW/kg)¹², meaning a TCA can deliver a force much larger
26 than its own weight (generally more than 100 times)¹³; 3) they can be directly driven by electricity
27 with a small voltage (a few volts)¹⁴; 4) they can sense their own deformation through the change
28 of electrical properties (e.g., resistance)^{15,16}. All of these characteristics will potentially enable
29 small-scale and untethered soft robots that in general are difficult to be accomplished by pneumatic
30 and tendon-driven methods^{17,18}. Further, unlike shape memory alloys, TCAs are intrinsically soft,
31 making it possible to embed them in any shape inside a soft body to generate versatile motion.

32
33
34
35
36
37 With the promising characteristics of TCAs, however, TCA-driven soft robots have been
38 scarce. In fact, only several rudimentary soft modules for crawling and bending are presented in
39
40
41
42
43
44
45
46
47
48
49
50
51
52
53
54
55
56
57
58
59
60

recent years¹⁹⁻²². The main reason is that traditional contraction TCAs' large stroke is generally obtained under a preload (e.g., a hanging weight). Without a preload, those TCAs will have negligible strokes because all the coils almost contact with each other. Such preloads will cause problems when TCAs are used to actuate soft robots since a preload will easily deform the soft body due to the low force bearing capability of soft materials (Young's modulus $10^4 \sim 10^9$ Pa)¹. For example, if we first preload a TCA by applying a stretching force before embedding it into a soft body, the tension force of the TCA will deform the soft body after removing the force. To address this problem, we can use an antagonistic configuration by using two TCAs in parallel, but it will require a larger force to bend, resulting in a small bending range²³. Note that TCAs that can extend generally do not need a preload, but they can only deliver much smaller forces compared with contraction ones²⁴.

In this paper, to better actuate soft robots with TCAs, we introduce a novel fabrication technique of contraction TCAs that will have uniform initial gaps between neighboring coils. In this case, they can contract over 48% without a preload, termed as *free stroke* in this paper. Such free strokes can enable soft robots by directly embedding one or multiple TCAs into a soft body without preloading those TCAs (Fig. 1a). With a large free stroke, TCAs can actuate the soft body to achieve a large magnitude of motion. They can also be arranged in different shapes inside a soft body to achieve programmable motions.

The main contributions of this paper are two-fold. First, we propose an [upgraded](#) fabrication method to generate TCAs with free strokes. Such TCAs can be applied to a wide variety of applications that requires artificial muscles, including robotics, haptics, intelligent structures, smart textiles, etc.²⁵. Second, we demonstrate soft robots with programmable motions by placing TCAs in different shapes inside a soft body. Specifically, we embed TCAs in a curved U shape, a

1
2
3 helical shape, and straight shapes in parallel to enable three different motions: two-dimensional
4 bending, twisting, and three-dimensional bending, respectively (Fig. 1b-d). We also combine the
5 three motions to demonstrate a completely soft robotic arm that mimics a human forearm (Fig. 1e
6 and f). Such demonstrations lay a foundation for achieving more complicated motion or shape
7 morphing by strategically embedding multiple TCAs inside a soft body, similar to recent results
8 using other actuation methods (e.g., pneumatic-driven²⁶ and liquid crystal elastomers^{27,28}). We
9 envision that this work will inspire a variety of TCA-driven soft/rigid robots or structures to
10 achieve versatile motions or morphologies, especially those in centimeter scales.
11
12
13
14
15
16
17
18
19
20
21
22
23

24 **2 Results and Discussion**

25
26

27 **2.1 TCAs with Free Strokes**

28

29 The fabrication process for TCAs with free strokes is built on the original mandrel coiling
30 process^{12,29} with a key difference: we coil a twisted thread on a special mandrel with a helical
31 groove, generating a coiled shape with uniform initial gaps between neighboring coils.
32
33
34
35

36 The major steps to fabricate a TCA with free strokes are shown in Fig. 2 (details in the
37 Supplementary Material Fig. s1 using our customized machine). First, a conductive sewing thread
38 is twisted to generate a twisted thread with the fiber pitch angle α_f and length l_0 (Fig. 2a).
39 Then, the twisted thread is coiled in the same direction as twisting on the special mandrel with a
40 helical groove that has a coil pitch angle α_m (Fig. 2b). The groove is formed by uniformly
41 wrapping a copper wire around a mandrel core (a cylindrical rod). With the groove, the twisted
42 thread will be guided into a helical shape with gaps between coils. Without the helical groove, the
43 twisted thread will not have gaps because the coils will be pulled together by a pulling force
44 generated by the internal untwisting torque in the thread (Fig. 2b). After the coiling process, the
45
46
47
48
49
50
51
52
53
54
55
56
57
58
59
60

1
2
3 coiled twisted thread is annealed in an oven with the helical mandrel whose two ends are fixed to
4 set this shape as an equilibrium state (Fig. 2c). After annealing, the coiled twisted thread can be
5 removed from the helical mandrel to generate a final TCA. A training process (several slow heating
6 cycles) needs to be applied before the first-time use to remove the TCA's internal stress to get
7 consistent performance ¹².
8
9

10 Using the proposed procedure, we fabricate five different TCAs according to two important
11 fabrication parameters (details in Supplemental Material TAB. s1): pitch angle during coiling (α_m, equals the pitch angle of the helical groove) and annealing temperature (T_a). We choose the
12 pitch angle because it will influence the initial gaps l_g between neighboring coils (Fig. 2b). In
13 fact, $l_g = 2 \tan(\alpha_m)(d_m + d_0)$, where d_m and d_0 are respectively the diameter of the mandrel
14 core, and the twisted thread (Fig. 2b and Fig. 3a). The annealing temperature will influence the
15 dynamic response of TCAs as will be presented in the next subsection. Note that we choose these
16 two factors because other fabrication parameters are easy to interpret or have been characterized
17 by others (e.g., the number of plies, the number of rotation inserted, the spring index, and different
18 materials ^{12,30}). We categorize the four TCAs according to the pitch angle α_m. For Type 1,
19 α_m = 15.57°, and Type 2, α_m = 22.54° (see Supplementary Material TAB. s1 for detailed
20 fabrication parameters). For each type, we anneal them under two temperatures (180 °C and 200
21 °C) and use a number after type number to indicate the temperature. For example, Type 1-180 is
22 annealed at 180 °C, while Type 1-200 is annealed at 200 °C.
23
24

25 Each of the four TCA has initial gaps between adjacent coils (Fig. 3a and b) that allow free
26 strokes without preloading. Each TCA exhibits a *natural length* l_n at room temperature when no
27 load is applied. It can achieve a minimum length l_{min} when heated, which is the length when all
28
29

1
2
3 coils contact (Fig. 3b). Therefore, the TCA can generate a reversible *free stroke* $S_f = (l_n - l_{min}) / l_n$
4
5 without a preload.
6
7

8 To demonstrate the free stroke, we actuate our TCAs using electricity to drag a weight
9 placed on a PVC sheet (Fig. 3c). The results show that a single TCA (Type 2-200 in TAB. s1) that
10 weighs only 0.03 g can overcome a peak friction force of 0.4 N to achieve a free stroke of
11 $S_f = 48\%$. By using 5 TCAs (weigh only 0.16 g) in parallel, we can drag a coffee kettle of 2 kg
12 to move 60 mm (Supplementary Video s1). *The maximum force that the TCA can generate before*
13 *breaking is 0.78 N (stress 8.59 MPa) when the two ends are fixed under the natural length.*
14
15

16 Our TCAs can also be used when a preload is applied (Fig. 3d) similar to conventional
17 TCAs without free strokes. In this case, the stroke is defined as $S = (l_{load} - l_{min}) / l_{load}$, where l_{load}
18 is the TCA's length after a load is applied. Results show that our TCA (Type 2-200) can generate
19 a stroke of 55% under 10 g load (Fig. 3d and Supplementary Video s2).
20
21

22 We compare our TCAs with several representative works^{12,22,23,30-35} in Tab. 1 by
23 categorizing them based on the coiling method: self-coiling (twist-induced coiling) and mandrel
24 coiling. In general, most of the existing TCAs have negligible free strokes because the coils contact
25 with each other after fabrication. For the strokes with preload, the largest stroke using the mandrel-
26 coiling method is 53%²³, and the largest stroke using the self-coiling method is 45%³⁵. The stroke
27 marked with * indicates that the stroke is normalized by l_n instead of l_{load} and will become
28 smaller when normalized with l_{load} .
29
30
31

51 2.2 Characterization of TCAs with Free Strokes

52
53

54 In this section, we experimentally characterize TCAs with free strokes through two steps.
55
56

1
2
3 First, we obtain the static response with respect to temperature and compare the results with
4 traditional TCAs without free strokes. We also explain the results using a model developed with
5 the system identification method. Second, we experimentally investigate dynamic response with
6 respect to time for the four TCAs with free strokes to choose one that will be suited for actuating
7 soft robots.
8
9
10
11
12
13

17 **2.2.1 Static response with respect to temperature**

18
19
20
21
22
23
24
25
26
27
28
29

To see why TCAs with free strokes are better than traditional TCAs, we fabricate a traditional TCA using a mandrel without the helical groove: Type 0-180. We compare its static response with the Type 1-180 with free strokes. To make proper comparisons, these two TCAs are made from the same twisted thread with the same parameters (details in Supplemental Material TAB. s1).

For these two TCAs, we perform static experiments by hanging a weight at the end of each TCA, slowly increasing the TCA's temperature in an oven, and recording the displacement (see Supplementary Material and Fig. s2 for details). Three TCAs that are separately fabricated are tested and their performance is pretty consistent because our TCA is fabricated with the customized, highly automatic machine. Therefore, only one TCA for each type is used throughout the systematic characterization. In the experiments, one experiment is repeated three times. Only the average of the three experiments are plotted in the following for a clear view and easy comparison, and the maximum standard deviation is 2.14 mm for Fig. 4a, b and c. The detailed measurement uncertainty (standard deviation) is reported in Section 5 of the Supplementary Material.

Experimental results of displacement with respect to temperature are plotted in Fig. 4a for

three different hanging weights: 0 g, 20 g, and 40. From the results, we can observe that all curves almost overlap with each other at the beginning, indicating they can be actuated similarly when the temperature is relatively low ($< 70^{\circ}\text{C}$) as observed previously by Haines et al¹² and Kianzad et al³⁶. However, all curves will flatten out as the temperature becomes high, suggesting the coils in TCAs are contacting each other to prevent further contraction. For different TCAs with the same weight, Type 1 can generate a larger displacement than Type 0, and the difference becomes larger as the weight increases. For instance, under 0 g (from 25 °C to 150 °C), Type 0 can contract 4 mm, while Type 1-180 can contract 20 mm. Note that Type 0 seems to contract more than 4 mm because the length of the TCA falls below the minimum length due to curling of its shape. But under 40 g (from 25 °C to 150 °C), Type 0 can contract only 24 mm, while Type 1-180 can contract 44 mm. For the same TCA under different weights, the case with the largest weight generates the most contraction since a heavier weight causes more gaps between coils. The

To better explain the difference between the traditional TCA and TCAs with free strokes, we can use a mathematical model to describe the relationship between temperature and the displacement³⁷:

$$F = k(l - l_n) + c\Delta T \quad (1)$$

where F is external load, k is the stiffness coefficient of the TCA, c is the force-temperature coefficient, l is the TCA's length, $\Delta T = T - T_0$ is the increase of temperature with T and T_0 the TCA's current and room temperature, respectively.

We can rearrange Eq. (1) to get the length in terms of temperature change

$$l = -\lambda\Delta T + l'_n, \quad l \geq l_{min} \quad (2)$$

where $\lambda = c/k$, and $l'_n(m) = F/k + l_n = mg/k + l_n$. We can use this equation to explain the performance difference for conventional TCAs and TCAs with free strokes in two different cases.

1
2
3 First, when $F = 0$, the conventional TCA almost cannot contract anymore since $l'_n = l_n \approx l_{min}$. But
4 for TCAs with free strokes, $l'_n = l_n > l_{min}$, there will be a free stroke, and it will contract to l_{min} at
5 a higher temperature. To see this, we plot the length with respect to temperature for the two TCAs
6 in Fig. 4b and c (figures with shaded error bars can be found in the Supplementary Material as Fig.
7
8 s4a and b). We also label the l_n and l_{min} in the figure. In these two figures, the blue shaded area
9 indicates the amount of the free stroke, and the TCA with free strokes can access a larger shaded
10 area compared with the conventional TCA. Second, for a fixed weight (i.e., $F \neq 0$),
11 $l'_n(m) = F / k + l_n$ will be larger for a TCA with free strokes since its k will be smaller under the
12 same fabrication conditions. In this case, TCAs with free strokes can also generate larger
13 displacements as can be seen from the five curves corresponding to 10, 20, 30, 40, and 50 g in Fig.
14 4b and c. We also approximate λ using a polynomial $\lambda = a\Delta T + b$ in terms of temperature, and
15 plot the fit results as dash-dotted lines, which match well with experimental results (See Section 5
16 of the Supplementary Material for details). However, the model does not capture the plateau part
17 of the experimental data; therefore it can only be used to predict the first part of the actuation. A
18 more sophisticated model could be developed by considering the contact of coils.

41 2.2.2 Dynamic response with respect to time

42
43 The static response for TCAs with free strokes indicates that the displacement largely
44 depends on the pitch angle during coiling (α_m). Besides static response, we also characterize how
45 the annealing temperature will influence TCAs' dynamic performance, which is critical if we want
46 to rapidly actuate soft robots, as most current TCA-driven soft robots are in general relatively slow.
47 For example, a soft bending module can only bend 60° after 10 s actuation and a crawling robot
48 can only move 1.2 % of its body length per second^{19,20} while the crawler actuated by shape
49
50
51
52
53
54
55
56
57
58
59
60

memory alloy wire can move over 200% of its body length per second with a rolling gait³⁸. For a given length of twisted thread l_0 in Fig. 2 a and b, a TCA's length after removing from the mandrel after annealing is around $l_m = l_0 \sin \alpha_m$. We call l_m the made length. But in general the natural length $l_n \leq l_m$ depending on the annealing temperature (T_a).

If T_a is below the Brill transition temperature of Nylon 6,6 (160 °C)³⁹, the TCAs, after removing from the mandrel, will automatically reduce its length until all gaps disappear to a minimum length given a sufficiently long time (several days) or subjected to a few heating cycles – a process called creep, which has also been observed by others³⁹. When T_a is higher than 160 °C and below 200 °C, the TCA will automatically creep to a natural length that is longer than its minimum length but shorter than the made length. For example, the natural lengths of Type 1-180 and Type 2-180 TCA are 92.5% and 80.5% of their made lengths (TAB. s1). The reason is that when the annealing temperature is low (e.g., less than 200 °C), the annealing process cannot fully remove the stress in the twisted thread. However, the TCAs annealed at 200 °C can almost maintain the made length (Fig. s3, Weight = 0). Therefore, the TCA's natural length will not only depend on the pitch angle during coiling, but also on the annealing temperature that determines the extent to which the TCA can hold the designed shape.

With the four TCAs with free strokes, we experimentally characterize their dynamic response under a constant weight (20 g) by applying a constant current (1 A) for 2 s to determine which one is better for actuating soft robots. Since these TCAs are fabricated with precursor threads of the same length, and thus resistance, they almost have the same temperature at the same time in the experiment. Fig. 4d plots the displacement with respect to time and the maximum standard deviation for the four curves is 2.12 mm, less than 4% of the TCA's maximum

displacement (60 mm). The results suggest that a TCA with $T_a = 200^\circ\text{C}$ (dash lines) can have a larger natural length, thereby a longer displacement upon actuation, but it has a slower time response compared with TCAs fabricated with $T_a = 180^\circ\text{C}$ (solid lines). In other words, TCAs annealed at 180°C (solid lines) can generate faster motion under the same actuation power compared with the TCA annealed in 200°C (dash lines). When we focus on the TCA annealed at 180°C (the solid lines), we observe that Type 1-180 TCA's (black solid line) contraction speed drops at a certain point, and its final displacement after 2 s is less than Type 2-180 TCA (red solid line). The reason is that it passes the natural length since Type 1-180 TCA (black solid line) has a shorter natural length than Type 2-180 TCA (red solid line). Among the four types of TCAs, Type 2-180 TCA (red solid line), which is annealed at a lower temperature but with a longer made length, is a better candidate for actuating soft robots since it actuates faster with a large displacement.

We also observe a *temporary natural length* due to the creep (viscoelasticity) of Nylon 66, the material of the threads used for fabricating TCAs with free strokes. Such a phenomenon is also mentioned in Ref^{40,41} for TCAs made of fishing lines. When a load is hanged at the end of a TCA, the length of TCA will first instantly increase due to the elastic stiffness of the spring structure and then gradually increase over time (Fig. s5b). After a TCA creeps to one length induced by a load, it takes a pretty long time in room temperature to return to its natural length after the load is removed (See Supplementary Material for more explanations and experimental verification). If TCAs are embedded into a soft body in these temporary natural lengths after the fabrication process, the TCA will eventually recover to its natural length, which will cause undesired initial deformation of the soft body. Therefore, we first conduct one heating cycle (in addition to the training process) before embedding the TCA into a soft body to prevent the undesired deformation.

1
2
3 Also, we tested the “aging” of the TCA (Type 1-180) by actuating it for 10,000 cycles (0.25 Hz)
4 at 2 MPa load, and the results show that the stroke changes little (2%, more detail in Section 7 of
5 the Supplementary material). The viscoelasticity might be also the reason for the hysteresis during
6 actuation and more sophisticated treatment can be found in other references^{42,43}.
7
8
9
10
11
12
13
14

15 **2.3 TCA-actuated Soft Robots with Programmable Motions**

16

17 The inherent softness of TCAs allows us to embed it with an arbitrary shape inside a soft
18 body to generate programmable and versatile motions. To demonstrate this, we embed TCAs in a
19 curved U shape, a helical shape, and straight shapes in parallel to enable three different motions:
20 two-dimensional bending, twisting, and three-dimensional bending, respectively. These three
21 motions represent typical ways to arrange soft artificial muscles in a 3D shape within a soft body
22 to achieve complex motion. Further, they can be combined together to generate a soft robotic arm
23 that mimics a human forearm to perform pick-and-place tasks (see section 2.4). For the results
24 presented below, we only use the same module throughout the experiments (the soft robotic arm
25 comprises the same module used in the characterization sections) to maintain consistency.
26
27
28
29
30
31
32
33
34
35
36
37
38
39
40
41
42
43
44
45
46
47
48
49
50
51
52
53
54
55
56
57
58
59
60

2.3.1 Two-dimensional Bending

We demonstrate two-dimensional bending motion with a soft gripper that is initially closed and can be opened by actuating an embedded TCA (Fig. 5a). We choose such a design strategy because the gripper can hold an object without consuming additional energy, whereas traditional soft grippers need to continuously consume energies when holding an object²⁴. Further, our design only requires a single TCA, simplifying the design and eliminating possible complicated position control for grasping⁴⁴.

The gripper is made of four parts: a curved U-shaped TCA (total length: 70 mm), a straight soft body (size: $35 \times 3 \times 5$ mm), one elastomer layer stiffer than the soft body, and one stretched (120%) elastomer layer (Fig. 5a). The soft body has two through holes to host the U-shaped TCA to generate uniform bending. The elastomer layer without prestretch serves as a strain limiting layer, while the one with prestretch bends the soft body to generate an initially closed shape. Such a fabrication allows us to avoid the difficulty to create channels with spatially curved U shape (See Supplementary Material for fabrication details).

To effectively use the proposed gripper for grasping objects with different sizes and weights, we need to address two questions: 1) how to open to different widths (d_w in Fig. 5b) so that it can grasp objects with different sizes; 2) how to determine the gripping force (F_g in Fig. 5c) it can generate at a given open width to make sure it can hold an object without additional energy input. We experimentally address these two questions. First, we evaluate how d_w will change with respect to the applied power for a fixed amount of time (2 s). The results shown in Fig. 5b (also Supplementary Video s3) indicate that d_w increases with respect to the input power, and the slope of the curve increases because the TCA displaces longer in the higher temperature region than in the low-temperature region as shown in Fig. 4d. To determine the gripping force, we drag the gripper open and record the displacement and force. Results in Fig. 5c suggest that F_g increases with respect to d_w , which means a larger opening will allow the gripper to hold a heavier object. The almost linear shape for the gripping force with respect to the opening width can be explained by possible analytical solution $w_d = cF_g$, where c is a constant determined by the geometry and material stiffness (assumed linear within a small range of deformation)⁴⁵.

The experimental results shown in Fig. 5b and c (The maximum standard deviations are

1
2
3 respectively 0.7990 mm and 0.085 N) can be used for guiding the grasping of an object. For an
4 object with a given size and weight, we can first determine if it is possible to hold it using results
5 in Fig. 5c (given a rough estimation of the friction coefficient). If it is possible to hold it, we can
6 use the results in Fig. 5b to apply a proper power to open the gripper to a width that is slightly
7 larger than the object's size. An example grasping process is shown sequentially in Fig. 5d with a
8 screwdriver. The gripper can also grasp different objects (a printed circuit board, a screw, and a
9 DC motor) with a variety of sizes and weights owing to the softness of the gripper (Fig. 5e and
10 Supplementary Video s3).

24 2.3.2 Twisting 25

26 To enable twisting motion, we wrap a TCA in a helical shape around a cylindrical soft
27 body (Fig. 6a). Before wrapping, the TCA is first inserted into an elastomer tube to protect the
28 TCA. We investigate two wrapping strategies using TCAs with the same total length (Fig. 6b) to
29 compare the twisting results: a single and double helix. A single helix is obtained by wrapping a
30 TCA uniformly along the soft body, while a double helix is fabricated by folding the TCA in half
31 before wrapping it on the soft body (See the Supplementary Material for fabrication details). To
32 make the twisting module compact (short), we wrap the TCA in both cases as close as possible.
33
34

35 To characterize the twisting motion, we record the twisting angle (ϕ) with respect to time
36 by applying the same power on the two different twisting modules (Fig. 6c), as well as different
37 power for the same amount of time (Fig. 6d). For the results shown in Fig. 6c, the constant power
38 is chosen as 28 W so that the double helix module can rotate around 180° in 2 s (See Supplementary
39 Video s4). The final twisting angle (ϕ) of the two designs gradually increases with respect to time.
40
41 As shown in Fig. 6c and d (the maximum standard deviations are both 6.3640 ° for the two
42

1
2
3 figures), the double helix one can rotate faster and realize a larger angle than the single helix one
4 under the same energy input (i.e., same actuation power for the same amount of time). This is
5 because the force generated by the double helix is almost twice the single helix for the same energy
6 input due to the small difference in their averaging wrapping angle (<10 degrees). So the single
7 helix module is limited by the force instead of displacement that a TCA can generate.
8
9
10
11
12
13
14
15
16

17 2.3.3 Three-dimensional Bending 18

19 We can also achieve three-dimensional bending motion by placing three TCAs in parallel
20 through three channels in a cylindrical soft body (Fig. 7a and Supplementary Video s5). By
21 properly actuating the three TCAs, we can bend the soft body towards a specific direction (bending
22 direction γ) with a specific amplitude (bending angle θ , Fig. 7b). To characterize how will γ
23 and θ change with respect to the input power for the three TCAs, we choose to apply different
24 powers to TCA1 and TCA2 since other combinations will be similar (TCA1 and TCA3, TCA2
25 and TCA3). The bending direction γ will be determined by the ratio of powers applied to TCA1
26 and TCA2, while bending angle θ will be determined by the magnitude of powers applied to
27 TCA1 and TCA2. Therefore, we perform two sets of experiments. In each set, we fix the power
28 applying to TCA2 P_2 , while change the power applied to TCA1 P_1 , thereby changing the power
29 ratio P_1 / P_2 . For the first set of experiments, $P_2 = 0.2$ W, and the ratio P_1 / P_2 changes from 1
30 to 5, while for the second set, $P_2 = 0.4$ W, and P_1 / P_2 varies in the same range.
31
32
33
34
35
36
37
38
39
40
41
42
43
44
45
46
47
48
49
50
51
52
53
54
55
56
57
58
59
60

To obtain γ and θ , we use a motion tracking system (Trio v120, OptiTrack) to track the
end position of the 3D bending module (marker 2, Fig. s8). In the simplest case [39], we can
assume the module has a constant bending curvature $\kappa = 1/r$ due to the relatively small weight

at the end. In this case, γ and θ can be solved from the end position of the module through the following minimization problem⁴⁶:

$$\begin{aligned} \min \quad & f(\gamma, \theta) = \| p - p' \| \\ \text{s.t.} \quad & \gamma \in [0, 90], \theta \in [0, 180] \end{aligned} \quad (3)$$

where

$$p' = [p'_x, p'_y, p'_z]^T$$

$$p = [p_x, p_y, p_z]^T = \frac{L}{\theta} [\sin \gamma (1 - \cos \theta), \cos \gamma (1 - \cos \theta), \cos \theta]^T$$

with p' the end position measured in experiments, p the end position represented using γ and θ , and L is the length of the module.

Figure 7c shows γ and θ change with respect to time under the same $P_2 = 0.4$ W but different power ratio (P_1 / P_2). The bending direction γ (solid lines) and the bending angle θ (dashed lines) increase with respect to time. The slope of θ is more influenced by the power ratio than γ . The increase of θ and γ is almost linear, though γ may decrease a little in the beginning. Figure 7d shows the final values of γ and θ with respect to the power ratio (P_1 / P_2) after applying electricity for 2 s. For the bending angle γ with the same P_2 , it increases with respect to the power ratio, meaning the module bends more towards TCA1. Also, the values for γ are approximately the same for the two different sets of experiments for the same power ratio, suggesting it indeed depends on the power ratio instead of the magnitude. For the bending magnitude θ , it increases with respect to the power ratio, similar to the trend for γ . But unlike γ , θ also depends on the magnitude of power. In fact, when the power ratio is the same, the bending magnitude θ for $P_2 = 0.4$ W can be much larger than the case with $P_2 = 0.2$ W. For

1
2
3 instance, θ is around 120° when $P_1 = 2$ W and $P_2 = 0.4$ W, whereas it is only around 50°
4
5 when $P_1 = 1$ W and $P_2 = 0.2$ W. Note that the applied power is relatively small compared with
6
7 the input for the twisting module since the 3D bending module has a much smaller bending
8 stiffness than the torsional stiffness. Also, due to the initial curved shape and inaccurate
9 measurement, θ may have a maximum initial error of 10° . The maximum standard deviation for
10
11 Fig 7. c and d are respectively 4.53° and 4.49° .
12
13
14
15
16
17
18
19
20
21
22
23
24
25
26
27
28
29
30
31
32
33
34
35
36
37
38
39
40
41
42
43
44
45
46
47
48
49
50
51
52
53
54
55
56
57
58
59
60

2.4 Combination of Modular Motions – A Soft Robotic Arm

We can combine the three modular motions (2D bending, twisting, and 3D bending) to develop a soft robotic arm: the gripper as a hand, the twisting module as a wrist, and the 3D bending module as an arm. Similar to the human's forearm, the robotic arm can achieve complicated motion and thus functions, for example, to pick and place an object by coordinating the three modules(Fig 1e and f). In our design, the arm is fabricated by connecting the gripper, the twisting module, and the 3D bending module in serial, with the end of the 3D bending module fixing to a base that can only move up and down (Fig. 8). The total weight of the arm is 6 g and the dimension is around $10 \times 10 \times 70$ mm.

Figure 8 and Supplementary Video s6 show the robotic arm can pick up different objects (a screwdriver and a PCB) and place them in different cups. In the process, the object is placed right under the arm with a known orientation. In this case, the wrist needs to first rotate some angles (around 45° with an input power of 14 W in Fig. 8a(i) and around 58° with input power of 16 W in Fig. 8b(i)) to align the gripper with the object. Then, according to the width of the object, the gripper opens different widths to grip the object (10 W in Fig. 8a(ii) and 8 W in Fig. 8b(ii)). After grasping the object, the wrist will return to its original orientation and the arm lifts

the object to some heights by moving up the base in Fig. 8a and b(iii). Then, the arm bends towards a desired cup ($P_1 = 0.6$ W, $P_2 = 0.6$ W in Fig. 8a(iv) and $P_1 = 0.2$ W, $P_2 = 0.8$ W in Fig. 8b(iv)). Finally, the arm releases the object by opening the gripper. Note that the 3D bending module can still bend noticeably (larger than 30 °) with the additional weight of the gripper, the twisting module, and the object.

3 Conclusion

In conclusion, this article presents TCAs with free strokes that are suitable for actuating soft robots. The TCA has an initial state with gaps between coils so that it can contract without preloading, generating around 50% free strokes that cannot be generated by traditional TCAs. We characterize its static response with respect to temperature and dynamic response with respect to time. The characterization results suggest that a relatively low annealing temperature and a large pitch angle during coiling can generate TCAs that respond faster with larger strokes. When embedding TCAs with free strokes into a soft body to build soft robots, we can achieve versatile, programmed motion, compared with previous work^{19,21,47}. We demonstrate individual modules for 2D bending, twisting, and 3D bending motion by properly arranging the TCAs in the soft bodies. By concatenating the individual modules, we build a first-ever miniature soft robotic arm actuated by TCAs. We demonstrate pick-and-place operations using the soft robotic arm. More complicated motion can be potentially achieved by arranging TCAs in other desired shapes. However, if the environmental disturbance (temperature, flow condition) is applied, to achieve the precise motion of the soft robots requires a closed-loop control.

Future work will focus on two aspects. First, we will establish both static and dynamic models for both TCAs with free strokes and TCA-actuated soft robots to predict and actively

control the resulting motion. This will be accomplished based on our previous efforts on the modeling of traditional TCAs²⁹ and TCA-actuated soft robots²⁴. Note that TCAs with free strokes necessitate new models since our previous models cannot work. Second, we will develop versatile soft robots for locomotion using TCAs with free strokes. Specifically, we will focus on underwater robots since heat dissipation is faster during the recovery process. By properly actuating several TCAs embedded in a soft body, we can potentially accomplish untethered soft robots with versatile motions, which currently is a bottleneck for soft robotics research¹⁷. Eventually, we envision that the [upgraded](#) TCAs can endow a variety of robots, soft or rigid, with large, programmable, and controllable motion in the future.

References

- [1]. Rus D, Tolley M T. Design, fabrication and control of soft robots. *Nature* 2015;521:467-75.
- [2]. Shepherd R F, Ilievski F, Choi W, *et al*. Multigait soft robot. *Proceedings of the national academy of sciences* 2011;108:20400-3.
- [3]. Calisti M, Giorelli M, Levy G, *et al*. An octopus-bioinspired solution to movement and manipulation for soft robots. *Bioinspiration & biomimetics* 2011;6:036002.
- [4]. Bartlett N W, Tolley M T, Overvelde J T, *et al*. A 3D-printed, functionally graded soft robot powered by combustion. *Science* 2015;349:161-5.
- [5]. Gu G-Y, Zhu J, Zhu L-M, *et al*. A survey on dielectric elastomer actuators for soft robots. *Bioinspiration & biomimetics* 2017;12:011003.
- [6]. Acome E, Mitchell S, Morrissey T, *et al*. Hydraulically amplified self-healing electrostatic actuators with muscle-like performance. *Science* 2018;359:61-5.
- [7]. Wehner M, Truby R L, Fitzgerald D J, *et al*. An integrated design and fabrication strategy for entirely soft, autonomous robots. *Nature* 2016;536:451.
- [8]. Miriyev A, Stack K, Lipson H. Soft material for soft actuators. *Nature communications* 2017;8:596.
- [9]. Wang C, Sim K, Chen J, *et al*. Soft ultrathin electronics innervated adaptive fully soft robots. *Advanced Materials* 2018;30:1706695.
- [10]. Wang W, Ahn S-H. Shape memory alloy-based soft gripper with variable stiffness for compliant and effective grasping. *Soft robotics* 2017;4:379-89.
- [11]. Huang X, Kumar K, Jawed M K, *et al*. Chasing biomimetic locomotion speeds: Creating

- untethered soft robots with shape memory alloy actuators. *Sci Robot* 2018;3.
- [12]. Haines C S, Lima M D, Li N, *et al*. Artificial muscles from fishing line and sewing thread. *science* 2014;343:868-72.
- [13]. Tawfick S, Tang Y. Stronger artificial muscles, with a twist. *Science* 2019;365:125-6.
- [14]. Mirvakili S M, Ravandi A R, Hunter I W, *et al*. Simple and strong: twisted silver painted nylon artificial muscle actuated by Joule heating. In: *Electroactive Polymer Actuators and Devices (EAPAD)* 2014; 2014.(pp. 90560I). International Society for Optics and Photonics.
- [15]. Abbas A, Zhao J. Twisted and coiled sensor for shape estimation of soft robots. In: *2017 IEEE/RSJ International Conference on Intelligent Robots and Systems (IROS)*; 2017.(pp. 482-7). IEEE.
- [16]. van der Weijde J, Vallery H, Babuška R J S r. Closed-Loop Control Through Self-Sensing of a Joule-Heated Twisted and Coiled Polymer Muscle. 2019.
- [17]. Rich S I, Wood R J, Majidi C. Untethered soft robotics. *Nature Electronics* 2018;1:102.
- [18]. Huang X, Kumar K, Jawed M K, *et al*. Soft Electrically Actuated Quadruped (SEAQ)—Integrating a Flex Circuit Board and Elastomeric Limbs for Versatile Mobility. *IEEE Robotics and Automation Letters* 2019;4:2415-22.
- [19]. Tang X, Li K, Liu Y, *et al*. A general soft robot module driven by twisted and coiled actuators. *Smart Materials and Structures* 2019;28:035019.
- [20]. Tang X, Li K, Liu Y, *et al*. A soft crawling robot driven by single twisted and coiled actuator. *Sensors and Actuators A: Physical* 2019;291:80-6.
- [21]. Yang Y, Tse Y A, Zhang Y, *et al*. A Low-cost Inchworm-inspired Soft Robot Driven by Supercoiled Polymer Artificial Muscle. In: *2019 2nd IEEE International Conference on Soft Robotics (RoboSoft)*; 2019.(pp. 161-6). IEEE.

- [22]. Almubarak Y, Tadesse Y. Twisted and coiled polymer (TCP) muscles embedded in silicone elastomer for use in soft robot. International Journal of Intelligent Robotics and Applications 2017;1:352-68.
- [23]. Wu L, Chauhan I, Tadesse Y. A novel soft actuator for the musculoskeletal system. Advanced Materials Technologies 2018;3:1700359.
- [24]. Pawlowski B, Sun J, Xu J, *et al.* Modeling of Soft Robots Actuated by Twisted-and-Coiled Actuators. IEEE/ASME Transactions on Mechatronics 2018;24:5-15.
- [25]. Mirvakili S M, Hunter I W. Artificial muscles: Mechanisms, applications, and challenges. Advanced Materials 2018;30:1704407.
- [26]. Siéfert E, Reyssat E, Bico J, *et al.* Bio-inspired pneumatic shape-morphing elastomers. Nature materials 2019;18:24.
- [27]. Kotikian A, Truby R L, Boley J W, *et al.* 3D printing of liquid crystal elastomeric actuators with spatially programed nematic order. Advanced Materials 2018;30:1706164.
- [28]. Aharoni H, Xia Y, Zhang X, *et al.* Universal inverse design of surfaces with thin nematic elastomer sheets. Proceedings of the National Academy of Sciences 2018;115:7206-11.
- [29]. Abbas A, Zhao J. A physics based model for twisted and coiled actuator. In: 2017 IEEE International Conference on Robotics and Automation (ICRA); 2017.(pp. 6121-6). IEEE.
- [30]. Haines C S, Li N, Spinks G M, *et al.* New twist on artificial muscles. Proceedings of the National Academy of Sciences 2016;113:11709-16.
- [31]. Li T, Wang Y, Liu K, *et al.* Thermal actuation performance modification of coiled artificial muscle by controlling annealing stress. Journal of Polymer Science Part B: Polymer Physics 2018;56:383-90.
- [32]. Yip M C, Niemeyer G. On the control and properties of supercoiled polymer artificial

- 1
2
3 muscles. IEEE Transactions on Robotics 2017;33:689-99.
4
5 [33]. Cho K H, Song M G, Jung H, *et al.* A robotic finger driven by twisted and coiled polymer
6 actuator. In: Electroactive Polymer Actuators and Devices (EAPAD) 2016; 2016.(pp. 97981J).
7
8 International Society for Optics and Photonics.
9
10 [34]. Kim K, Cho K H, Jung H S, *et al.* Double helix twisted and coiled soft actuator from
11 spandex and nylon. Advanced Engineering Materials 2018;20:1800536.
12
13 [35]. Yang S Y, Cho K H, Kim Y, *et al.* High performance twisted and coiled soft actuator with
14 spandex fiber for artificial muscles. Smart Materials and Structures 2017;26:105025.
15
16 [36]. Kianzad S, Pandit M, Bahi A, *et al.* Nylon coil actuator operating temperature range and
17 stiffness. In: Electroactive Polymer Actuators and Devices (EAPAD) 2015; 2015.(pp. 94301X).
18
19 International Society for Optics and Photonics.
20
21 [37]. Masuya K, Ono S, Takagi K, *et al.* Nonlinear dynamics of twisted and coiled polymer
22 actuator made of conductive nylon based on the energy balance. In: 2017 IEEE International
23 Conference on Advanced Intelligent Mechatronics (AIM); 2017.(pp. 779-84). IEEE.
24
25 [38]. Lin H-T, Leisk G G, Trimmer B. GoQBot: a caterpillar-inspired soft-bodied rolling robot.
26 Bioinspiration & biomimetics 2011;6:026007.
27
28 [39]. Rafie Ravandi A. Characterizing the behavior of nylon actuators and exploring methods for
29 manufacturing them to get the highest amount of output: University of British Columbia; 2018.
30
31 [40]. Cherubini A, Moretti G, Vertechy R, *et al.* Experimental characterization of thermally-
32 activated artificial muscles based on coiled nylon fishing lines. Aip Advances 2015;5:067158.
33
34 [41]. Huang Y-W, Lee W-S, Chuang Y-F, *et al.* Time-dependent deformation of artificial
35 muscles based on Nylon 6. Materials Science and Engineering: C 2019;98:445-51.
36
37 [42]. Zhang J, Simeonov A, Yip M C. Three-dimensional hysteresis compensation enhances
38
39
40
41
42
43
44
45
46
47
48
49
50
51
52
53
54
55
56
57
58
59
60

- accuracy of robotic artificial muscles. *Smart Materials and Structures* 2018;27:035002.
- [43]. Konda R, Zhang J. The Effects of Nylon Polymer Threads on Strain-Loading Hysteresis Behavior of Supercoiled Polymer (SCP) Artificial Muscles. In: ASME 2019 Dynamic Systems and Control Conference. American Society of Mechanical Engineers Digital Collection.
- [44]. She Y, Li C, Cleary J, *et al.* Design and fabrication of a soft robotic hand with embedded actuators and sensors. *Journal of Mechanisms and Robotics* 2015;7:021007.
- [45]. Zhu Z, Meguid S. Elastodynamic analysis of low tension cables using a new curved beam element. *International journal of solids and structures* 2006;43:1490-504.
- [46]. Webster III R J, Jones B A. Design and kinematic modeling of constant curvature continuum robots: A review. *The International Journal of Robotics Research* 2010;29:1661-83.
- [47]. Sun J, Pawlowski B, Zhao J. Embedded and controllable shape morphing with twisted-and-coiled actuators. In: 2018 IEEE/RSJ International Conference on Intelligent Robots and Systems (IROS); 2018.(pp. 5912-7). IEEE.

Reference	Precursor Fiber	Coiling	Spring Index	Free Stroke	Stroke	Load for Stroke
Haines et al [12]	Fishing Line	Mandrel	5.1	NA	49%	1 Mpa
Haines et al [30]	Fishing Line	Flat Spiral	NA	NA	46%	NA
Wu et al [23]	Fishing Line	Mandrel	5.2	NA	53%	100g (1.8 Mpa)
Li et al [31]	Fishing Line	Self-coiling	NA	NA	18% *	100 g
Yip et al [32]	Conductive Thread	Self-coiling	NA	NA	10%	200 g
Cho et al [33]	Conductive Thread	Self-coiling	NA	NA	17.8%	1000 g
Almubarak et al [22]	Conductive Thread	Self-coiling	NA	NA	22% *	200 g
kim et al [34]	Spandex & Conductive Thread	Self-coiling	NA	NA	40.1%	1.9 N
Yang et al [35]	Spandex	Self-coiling	NA	NA	45%	60 g
Our Work	Conductive Thread	Helical Mandrel	3.5	48%	55%	10 g

TAB. 1 Comparison of TCAs' strokes with representative works

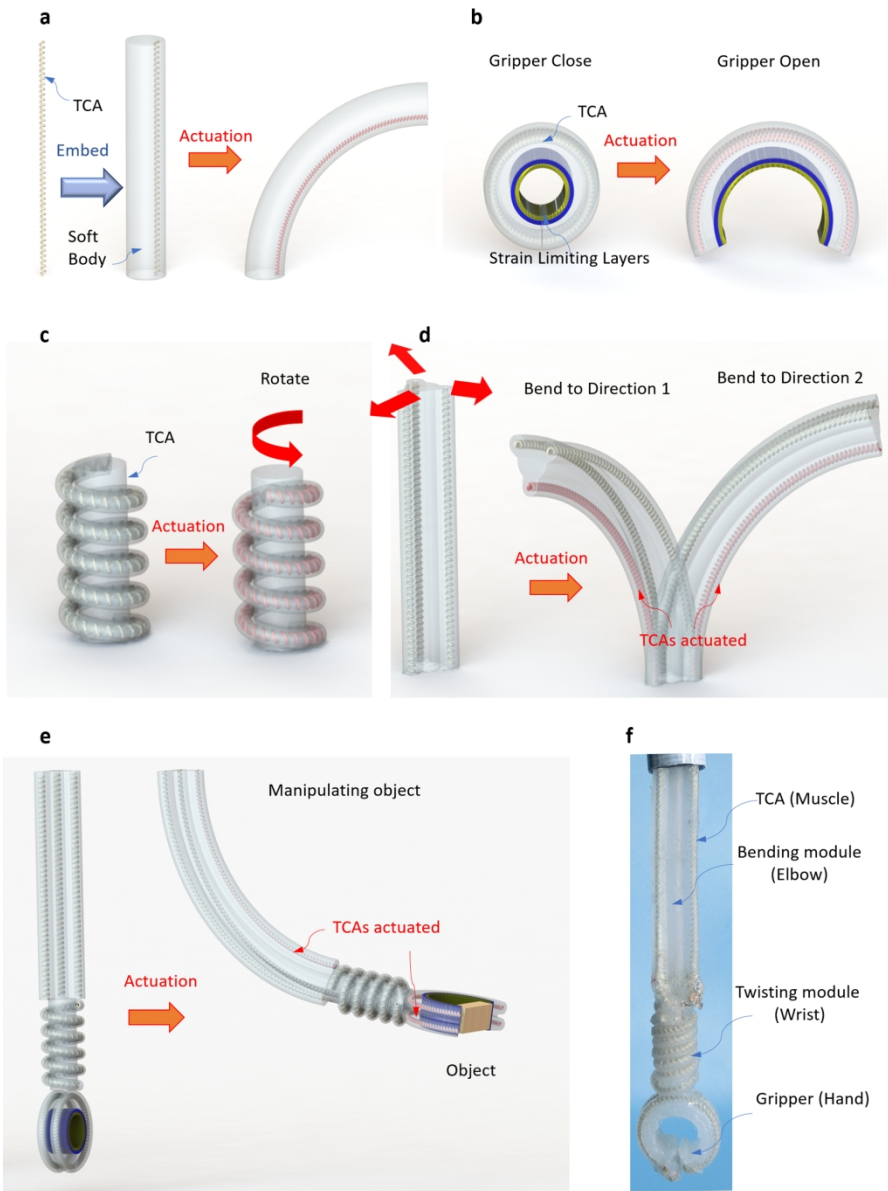


Figure 1: TCAs with free strokes can enable programmable motions for soft robots. (a) TCAs with free strokes can be directly embedded into a soft body to generate a large bending angle when actuated. (b)-(d) Versatile motions generated by arranging TCAs in soft bodies. (b) A 2D bending module (gripper) with TCA in a curved U shape. (c) A twisting module with a TCA in a helical shape. (d) A 3D bending module with 3 TCAs in parallel. (e) The schematic of a soft robotic arm with a 3D bending module, twisting module, 2D bending module. (f) A prototype of the soft robotic arm.

170x227mm (300 x 300 DPI)

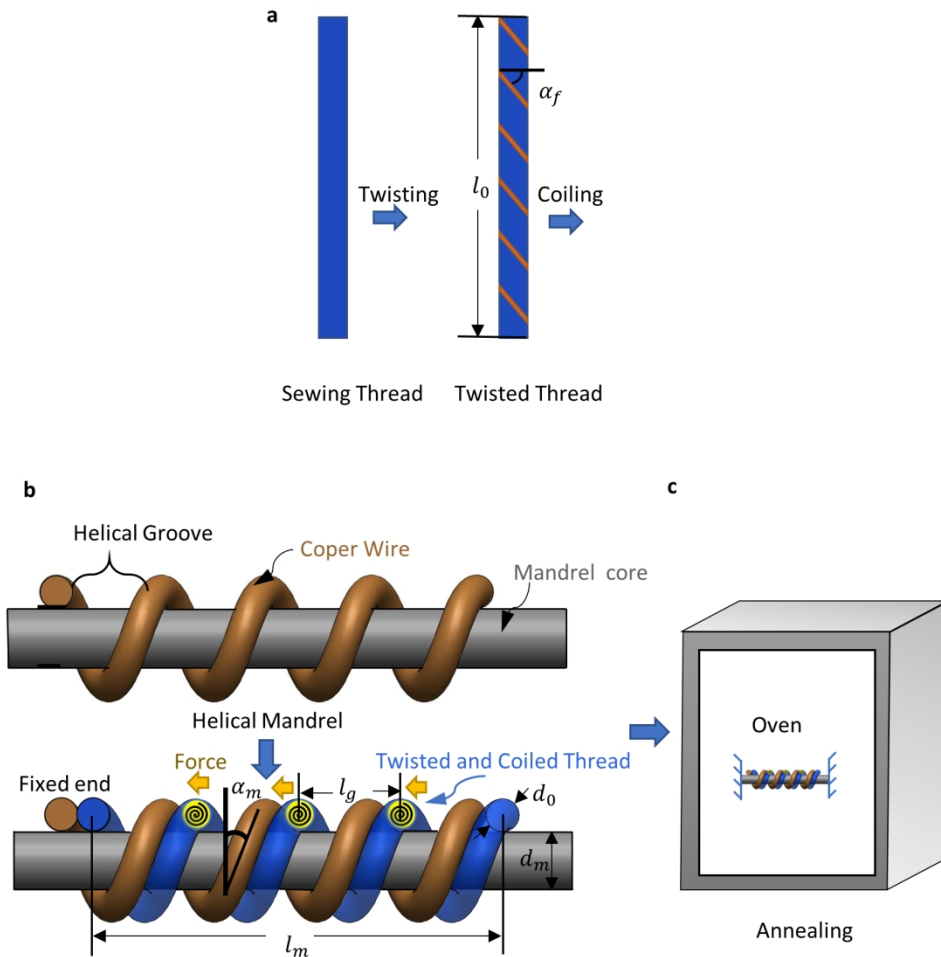


Figure 2: The schematic showing the fabrication process of TCAs with free strokes. (a) Twist a sewing thread to generate a twisted thread. (b) Coil the twisted thread on a helical mandrel with a cylindrical mandrel core and helical grooves formed by a copper wire to generate coiled and twisted thread. (c) Anneal the coiled and twisted thread in an oven to generate the final Twisted-and-Coiled Actuator (TCA).

163x163mm (300 x 300 DPI)

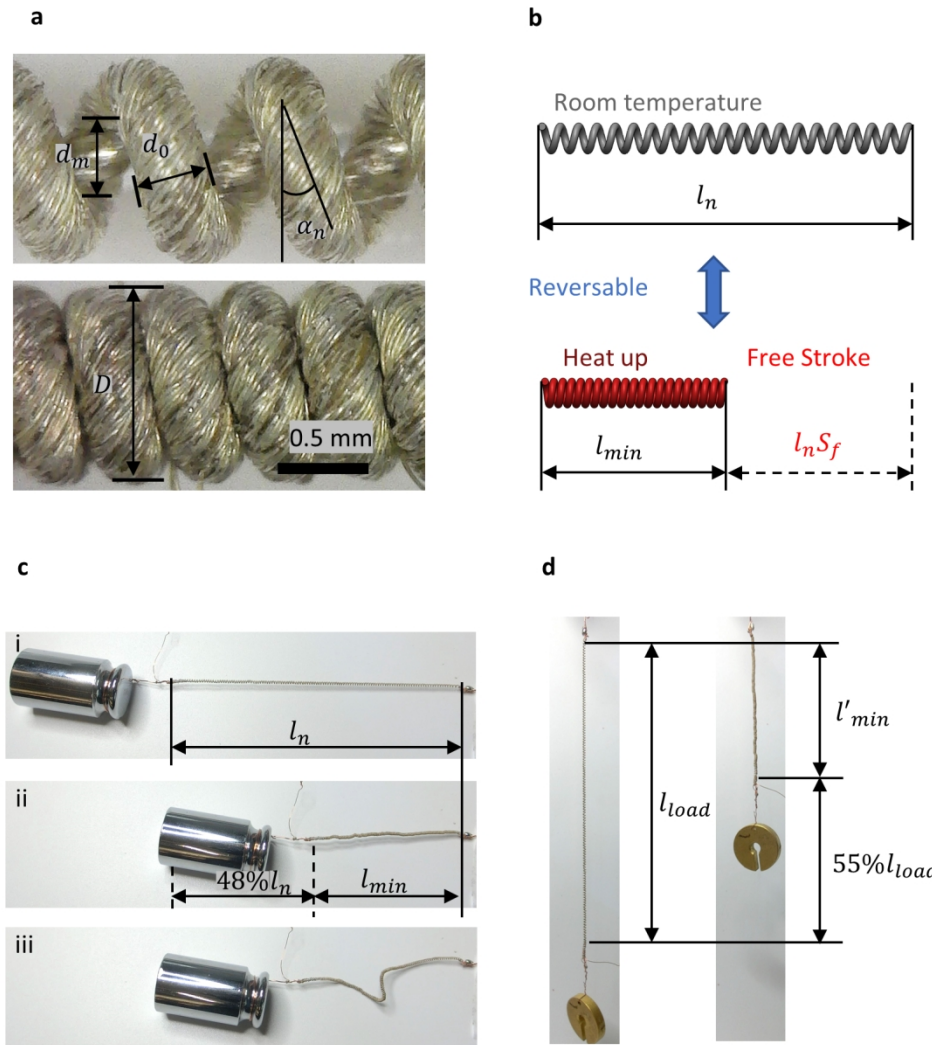


Figure 3: Our proposed TCAs can contract without preloading (a) Microscopic photos of the TCA in room temperature (top) and after being heated up (bottom). (b) Schematic of the TCA illustrating natural length l_n , minimum length l_{min} , and the free stroke S_f . (c) The TCA pulls a weight against friction of 0.4 N to generate a free stroke of 48%. (d) The TCA lifts a weight of 10 g against gravity to generate a loaded stroke of 55%.

145x160mm (300 x 300 DPI)

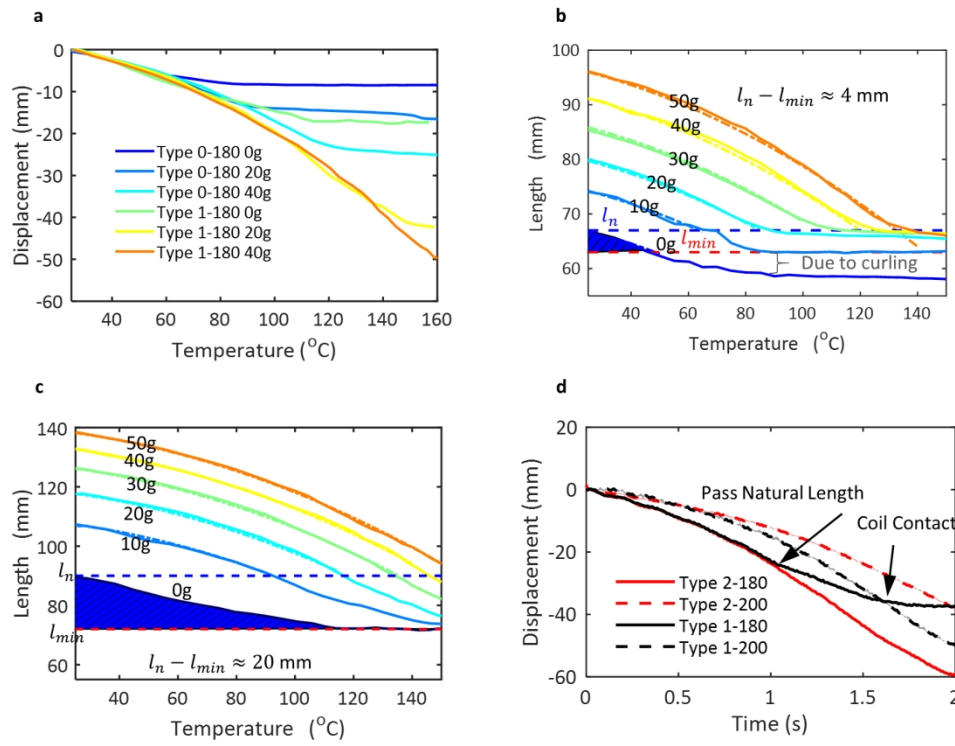


Figure 4: Characterization of the static response with respect to temperature for a conventional TCA (Type 0) and a TCA with free strokes (Type 1). (a) The displacement with respect to temperature under different weights. (b) The experimental (solid lines) and fitted (dash-dotted lines) results of a conventional TCA's (Type 0) length with respect to temperature. (c) The experimental (solid lines) and fitted (dash-dotted lines) results of the TCA's (Type 1) length with respect to temperature. The figures with shaded error bars can be found in Fig. s 4 a and b of the Supplementary Material. (d) The dynamic response with respect to time for four different TCAs with free strokes when actuated by a constant current (1 A) under the same load (20 g).

Type 2-180 (red solid line) responds faster with a large displacement. The lines indicate the average and shaded regions indicate the standard deviation. The maximum standard deviation for the four curves is 2.12 mm.

164x128mm (300 x 300 DPI)

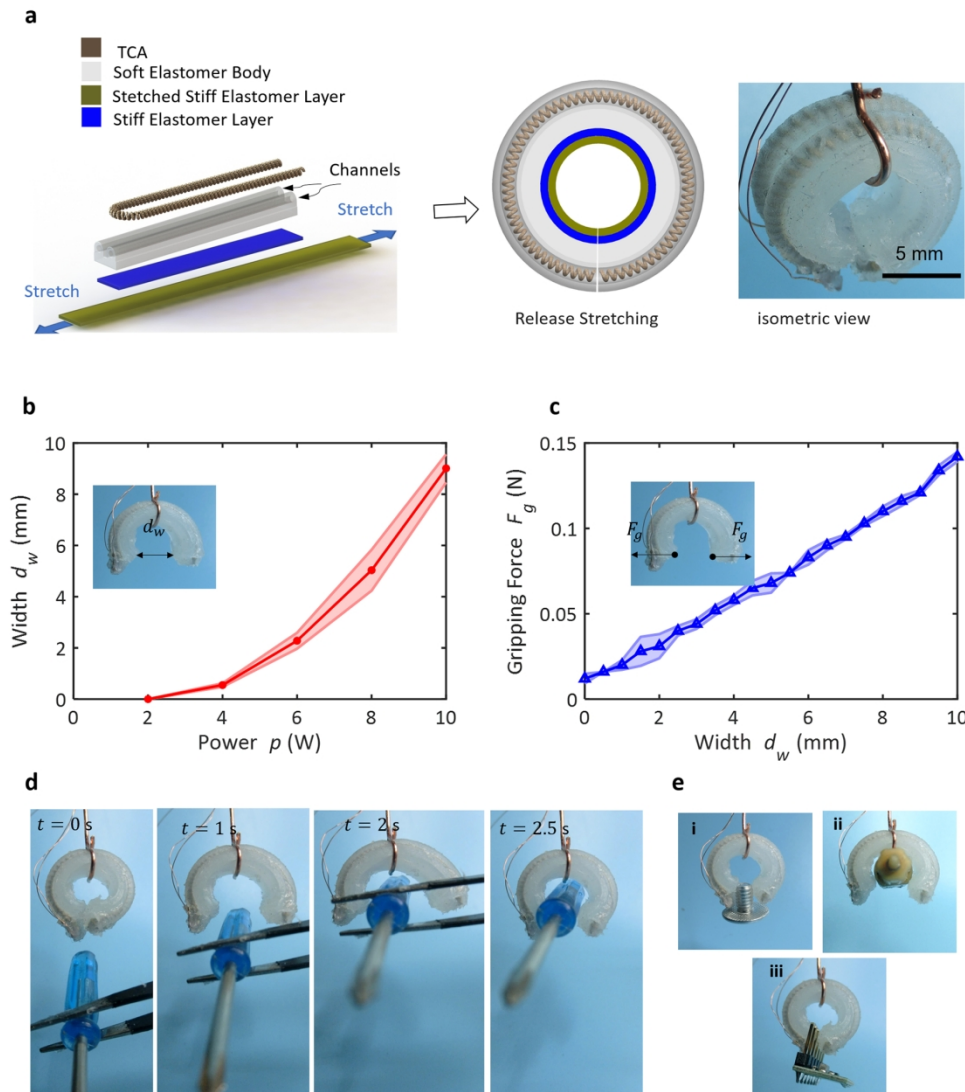


Figure 5: Two-dimensional bending motion manifested by a gripper which is normally closed and can be opened by actuating an embedded TCA. (a) The fabrication schematic of the gripper and an isometric view. (b) The opening width of the gripper when different power is applied for 2 s. Solid lines indicate the average and shaded regions indicate the standard deviation. The maximum standard deviation is 0.7990 mm. (c) The gripping force of the gripper with respect to the opening width. The maximum standard deviation is 0.085 N. (d) An example gripping process of a screwdriver. Electricity is applied at $t = 0$ s, the gripper opens wide enough at $t = 2$ s. Finally, at $t = 2.5$ s, the gripper closes and holds a screwdriver. (e) Several objects that the gripper can grasp: i. a metal screw. ii. a small DC motor. iii. a printed circuit board.

160x177mm (300 x 300 DPI)

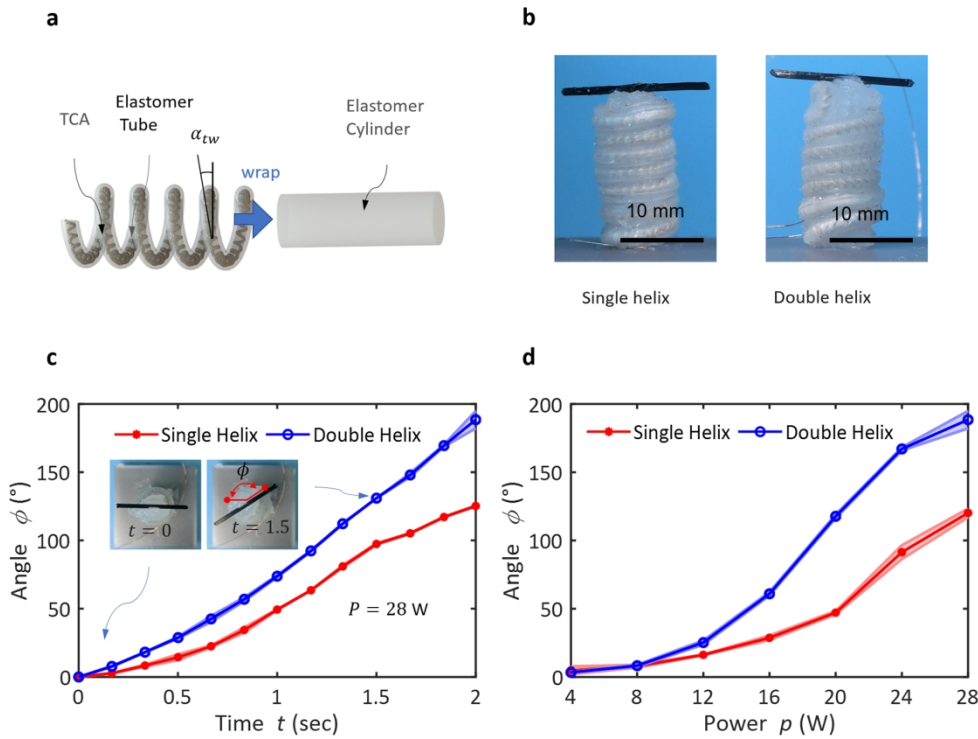


Figure 6: Twisting motion generated by wrapping a TCA around a cylindrical soft body. (a) The schematic of fabricating the twisting module. (b) The twisting module with two different wrapping strategies: single helix or a double helix. (c) The twisting angles ϕ of the twisting module with respect to time when a power of 28 W is applied with maximum . (d) The twisting angle of the two modules after applying different power for 2 s. The lines indicate the average and shaded regions indicate the standard deviation and the maximum standard deviations are both 6.3640° for (c) and (d)

160x122mm (300 x 300 DPI)

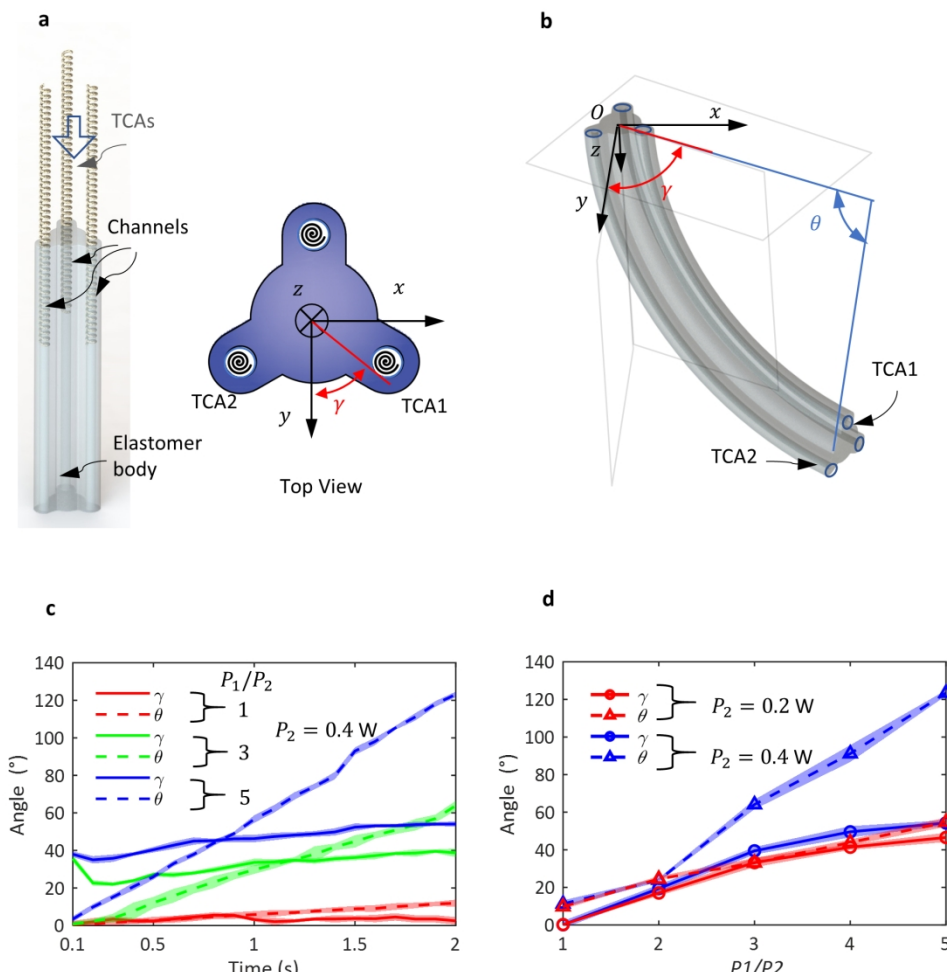


Figure 7: 3D bending motion generated by three TCAs placed in parallel in a soft body. (a) The schematic to fabricate the 3D bending module with the top view shown on the right. (b) A three-dimensional schematic showing bending direction γ and the bending angle θ . (c) The bending angle and the bending direction with respect to time. (d) The bending angle and the bending direction with respect to input power ratio for two cases $P_2 = 0.2$ W and $P_2 = 0.4$ W . For both (c) and (d), the lines indicate the average and shaded regions indicate the standard deviation. The maximum standard deviation of all curves for (c) is 4.53° and for (d) is 4.49° .

177x181mm (300 x 300 DPI)

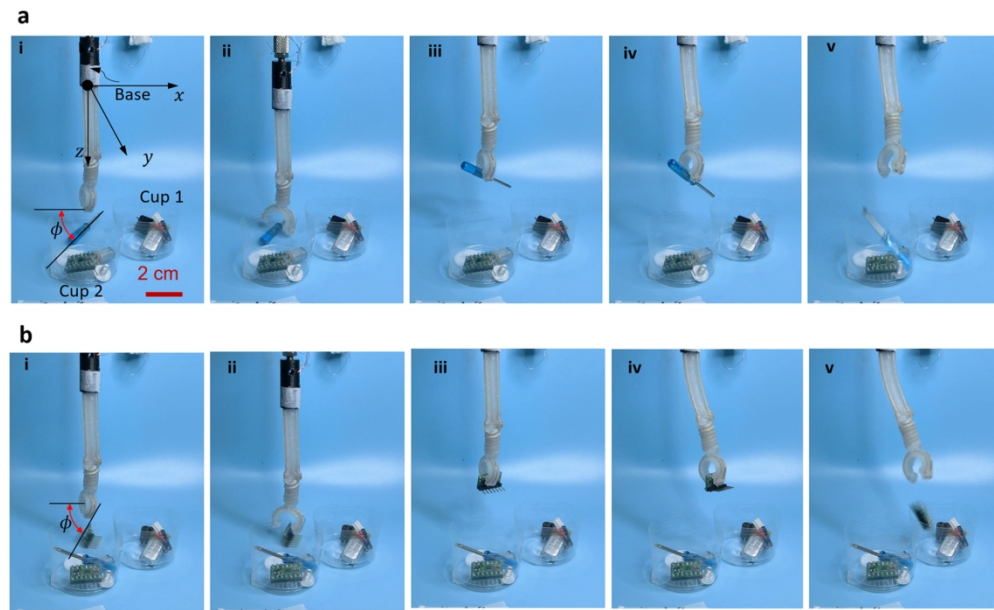


Figure 8: A soft robotic arm that can perform pick-and-place tasks. (a) and (b) i. The object is placed under the gripper. ii. The gripper opens and rotates when the arm approaches the object. iii. The gripper grasps the object and lifts it to a certain height. iv. The arm bends towards the target cup. v. The gripper releases the object into the cup.

NO.	α_m	α_n	l_m	l_n	S_f	T_a
Type 0-180	11.53	10.8	70	61	5.7%	180
Type 1-180	15.57	14.56	94	88	20.4%	180
Type 2-180	22.54	18.14	133.5	109	35.7%	180
Type 1-200	15.57	15.57	96	96	27.2%	200
Type 2-200	22.54	22.54	134	134	48%	200

TAB. s1 The fabrication parameter of TCAs

Supplementary Material

Jiefeng Sun, Brandon Tighe, Yingxiang Liu, and Jianguo Zhao

1 **The customized machine for fabricating TCAs with free strokes**

We design a customized machine to fabricate TCAs with free strokes as shown in Fig. s1a. The machine has two step motors A and B (coiling motors) facing each other in a horizontal line and a traveler controlled by another step motor C (guiding motor) that can travel between the two motors. The two coiling motors are used to hold a mandrel core (a cylindrical rod or wire) and apply a tension to keep the mandrel taut. The traveler is used to guide a copper wire wrapped on the mandrel core to form a helical groove. The main function of the machine is to fabricate a helical mandrel and coil a twisted fiber on the mandrel in the guiding groove. The machine can fabricate a TCA that has a maximum length of 350 mm in 8 mins except for the annealing and training time.

2 **Fabrication of the helical mandrel**

To fabricate the helical mandrel, we first tie the two ends of a rigid carbon fiber rod to the two coiling motors' shafts (Fig. s1a). A copper wire travels with the traveler at a constant speed from one end to the other. When the two motors are rotating in the same direction, the copper wire will be wrapped around the carbon rod in a helical shape to form the guiding groove. After

1
2 that, we fix the two ends of the copper wire on the carbon rod and a firm groove will be formed
3 on the mandrel. The speed ratio between the guiding motor and the coiling motors can be tuned
4 to fabricate a helical mandrel with different coil bias angles.
5
6
7
8
9
10
11

3 Fabrication of TCAs with free strokes

15 Then, we fabricate TCAs with free strokes by coiling a twisted fiber on the helical mandrel
16 along the groove. In Fig. s1b, We twist 1 thread (Shieldex Trading, 235/36 dtex 4 ply HC+B)
17 with an initial length of 350 mm by hanging a weight of 240 g, and the process ends after
18 inserting $N = 287$ rotations before auto-coiling starts. A weight heavier than 240 g may easily
19 break the threads and a lighter weight will not allow for enough twisting of the threads. Fig.
20 s1c shows that the both motors rotate the helical mandrel to coil the twisted threads on it along
21 the groove in the same direction as twisting. After that, the two ends of the twisted threads
22 are clipped on the mandrel to prevent it from uncoiling. The actuator is then annealed in an
23 oven (Quincy Lab 10GCE, accuracy 0.5°C) for 2.5 hours at a temperature of 180°C or 200°C.
24 Finally, we obtain a stabilized TCA that does not untwist when the copper wire is unwrapped
25 from the carbon fiber rod (Fig. s1 d-e).
26
27
28
29
30
31
32
33
34
35
36
37
38
39
40
41

42 After the TCA is removed from the mandrel core, a training process in Fig. s1f is performed
43 to endow the TCA a reversible stroke. In the process, a weight of 2 g is hanged at the end of
44 the TCA to keep it straight, and we apply electricity to make it fully contracted for 10 times.
45 Finally, the TCA will have a reversible stroke (free stroke) and recover to a certain length even
46 without any external load after cooling. The length of the TCA after training (natural length
47 in main texts) will be shorter than the length when it is with the mandrel (called made length
48 in main texts). We can easily fabricate TCAs with different parameters. For example, we can
49 fabricate TCAs with different inner diameters and coiling angles by changing the diameter of
50 the carbon fiber rod and traveling speed of the traveler. We totally fabricated 5 types of TCAs
51
52
53
54
55
56
57
58
59
60

1
2 using the same twisting fiber and their parameters are summarized in TAB. s1.
3
4

5 With the machine, it takes total 8 mins to fabricate the TCA: 3 mins to fabricate one helical
6 mandrel, 3 mins to fabricate a twisting thread and another 2 minutes to coil the twisted threads
7 on the mandrel. To improve efficiency, a long TCA could be fabricated and cut into several
8 pieces for different usages.
9
10
11
12

13 14 15 16 17 4 Fabrication parameters of TCAs used in this work

18 19 20 21 The five TCAs (type 0, type 1, and type 2) have the following same parameters
22
23

24 d_0 : Diameter of the twisted thread (after twisting), 0.34 mm

25 d_m : The diameter of the mandrel core (equals to the inner diameter of the TCA), 0.405 mm

26 D : Outer Diameter of the TCA, 1.08 mm

27 C : Spring index $C = D/d_0 = 2.17$

28 l_0 : Initial twisted thread length, 350 mm

29 30 31 32 33 34 35 36 37 38 39 40 The five TCAs (type 0, type 1, and type 2) have the following parameters with different
values listed in TAB. s1). Note that the pitch angle during coiling for conventional TCA without
free strokes (Type 0) cannot be changed.

41 42 43 44 45 α_m : pitch angle during coiling process, °(Note that this angle is equal to the pitch angle of
the helical groove)

46 47 48 α_n : pitch angle corresponding to the natural Length, °

49 l_m : Made length, mm

50 51 l_n : Natural Length, mm

52 53 54 S_f : Free stroke, $S_f = (l_n - l_{min})/l_n$

55 56 57 T_a : Annealing temperature, °C

NO.	α_m	α_n	l_m	l_n	S_f	T_a
Type 0-180	11.53	10.8	70	61	5.7%	180
Type 1-180	15.57	14.56	94	88	20.4%	180
Type 2-180	22.54	18.14	133.5	109	35.7%	180
Type 1-200	15.57	15.57	96	96	27.2%	200
Type 2-200	22.54	22.54	134	134	48%	200

18 TAB. s 1. Parameters of different types of TCAs fabricated in the paper
 19

23 5 Experiments for static response with respect to temperature

26 First, the TCA is placed in the oven that is used to fabricate the TCA (Fig. s2). Its top is
 27 fixed to the oven and its bottom is connected to a carbon fiber rod that comes out from the vent
 28 hole of the oven. We place a marker at the top of the carbon fiber rod and use a laser sensor
 29 (OPT2006, Wenglor sensoric GmbH) to monitor the contraction of the TCA. The weight of the
 30 carbon fiber rod with the marker is only 0.2g. In an experiment, a specific weight (one of 0 g,
 31 32 33 34 35 36 37 38 39 40 41 42 43 44 45 46 47 48 49 50 51 52 53 54 55 56 57 58 59 60 10 g, 20 g, 30 g, 40 g, and 50 g) is hanged at the bottom of the TCA.

40 In the experiment, the temperature of the oven gradually increases to 160°from the room
 41 temperature in around 14 mins and the temperature is recorded with a thermistor (EPCOS Inc.,
 42 B57540G0503F000, time constant 3s). Due to the comparable sizes of the TCA and the ther-
 43 mistor and the low increasing rate of the temperature, we can treat the temperature of the TCA
 44 is approximately the temperature measured by the thermistor. Before an experiment, we place
 45 the corresponding weight and conduct a heating cycle using electricity and wait 3 mins to start
 46 an experiment. This will allow the TCA to quickly creep to a length close to the steady state
 47 length corresponding to the weight, which is shown in Fig. s3. **The maximum standard devi-**
 48 **ates for the 6 measurements (0g, 10g, ..., 50g) for the Type 0-180 (Fig. s4a) are respectably**

1
2 0.6623, 0.3615, 1.6505, 1.6360, 0.8487, and 0.3535 mm and for the Type 1-180 (Fig. s4b) are
3 respectively 1.8909, 1.4810, 1.6113, 1.6045, 1.6045, and 2.1412 mm
4
5
6
7
8

9 **6 Parameter identification of TCA's displacement-temperature rela-** 10 **tionship** 11 12

13 Based on our observations, the tailored TCAs' displacement cannot be described using a
14 linear model, where both c and k are constant. Therefore, we approximate λ using a polynomial
15 $\lambda = a\Delta T + b$ in terms of temperature. The value of a and b can be found using a least-square
16 fit, $a = 0.0012 \text{ mm/K}^2$, $b = 0.140 \text{ mm/K}$. We can see this model can match the experiments
17 very well before the coils becoming too close.
18
19

20 Since the length changes with respect to time due to creep (Fig. S3), k is dependent on the
21 TCA's time as well as length. To avoid modeling creep, we direct measure l'_n and use it as a
22 modeling parameter. The simulated results are plotted in Fig.4 (a) and (b) as dash-dotted lines,
23 which also match well with experimental results.
24
25
26

27 **7 Temporary length and aging test** 28 29

30 **Temporary Length** 31 32

33 Our TCAs with free strokes exhibit a temporary length right after fabrication or subject to an
34 external load due to the creep of polymer materials. After the annealing process and removing
35 from the mandrel, it will slowly (around one day) creep to its natural length from a *temporary*
36 *natural length* (slightly shorter than the made length). Such a creeping process can be sped up
37 by several heating cycles. Therefore, we apply 10 heating cycles before we embed a TCA into
38 a soft body when fabricating soft robots to make sure the TCA has a natural length instead of a
39 temporary natural length.
40
41
42
43
44
45
46
47
48
49
50
51
52
53
54
55
56
57
58
59
60

When subject to an external load, the TCA also exhibits a temporary length. We conduct an experiment to demonstrate the temporary length. In the experiment, a Type 1-180 TCA is hanged and a motion tracking system (OptiTrack, V120:Trio) is used to track the length change of the TCA by sticking two markers at its two ends (see inset in Fig. s5a). Fig. s5a shows the TCA's length with respect to time. At the beginning, the TCA is at its natural length $l_1 = l_n$ with no load at the end. Then a weight $m = 20$ g is hanged at its end, and the length becomes l_2 due to the instant elastic deformation. After a heating cycle is applied, the length starts to creep to l_3 after the TCA cools down for about 100 s. Also, when we remove the weight, the TCA's length (becomes l_4) will not able to immediately recover to the natural length l_1 . The creeping effect will temporally keep the TCA's length, which is a *temporary length*. Finally, the length recovers to l_1 after we apply another heating cycle. We find $l_1 < l_2 < l_4 < l_3$, and the difference between l_2 and l_3 is not only due to instant elastic deformation but due to creep, which is accelerated by the heating process. In another experiment, we first hold a weight of 20 g with hands when the TCA is at its natural length l_1 . Then, we suddenly release the weight, the length will first instantly increase to a length l_2 , and finally creep to a steady-state length after tracking the length of the TCA for 20 hours as in Fig. s5b. When we remove the weight, it takes also the same amount of time to recover to the natural length.

Aging Test

The setup that is used for measuring the temporary length is used again in this test. We hang a weight of 20g (2 MPa) at the end of the TCA (Type 1-180) and actuate it at 0.25 Hz for 10,000 cycles. Fig. s6 provides the stroke as a function of cycle (each point averages 100 cycles). The results show that the long-time creeping of the stroke is around 2% after 10,000 cycles.

8 General fabrication procedures for TCA-actuated soft modules

Instead of directly embedding the TCA in the curing process, we fabricate them by assem-

1
2 bling the TCA and the soft bodies together afterward. The detailed fabrication procedures for
3 all the TCA-actuated soft modules are as following: 1) Fabricate soft bodies with channels. 2)
4 Assemble TCA in the soft bodies. 3) Connect electrical leads to the TCA. 4) Reshape the soft
5 bodies. 5) Assemble the soft bodies together.
6
7
8
9
10

11 Fabricate soft bodies with channels. We use the same elastomer (Ecoflex 30, Smooth-On
12 Inc.) for all of our soft robots in this study. Its pre-polymer mixture is prepared in three steps:
13 (i) mixing the two components, A and B, in a 1:1 ratio, (ii) manually stirring them for ~5 min,
14 and (iii) degassing the mixture under vacuum for ~10 min. Then the mixture is poured into a
15 mold with carbon fiber rods (diameter 0.9 mm) that are used to create channels as shown in Fig.
16
17 s7.
18
19
20
21
22
23
24
25

26 Assemble TCA in channels. Based on the length of channels in a soft body, we first de-
27 termine the required length for a TCA. After that, in each fabrication, we cut a TCA into the
28 required length to make sure the fabrication to be uniform. Then the TCA is sewed into the soft
29 body (for example, the body in the twisting manipulator is the tube) passing through the chan-
30 nels. To reduce the friction between the soft body and the TCA, **oil (3-IN-ONE Multi-Purpose**
31 **Oil)** is used to lubricate the channels. **Note that oil is only to hlep the assembling process and**
32 **it is not necessary when TCA is working in the soft body.** This assembly method allows more
33 flexibility to arrange multiple TCAs, because we can fabricate a soft body with channels in
34 simple geometry and arrange it to a complex shape when assembling (e.g., a helical shape).
35
36
37
38
39
40
41
42
43
44
45
46
47
48
49
50
51
52
53
54

55 Connect electrical leads. Two copper wires are connected to the ends of the TCA. After
56 that, we fix the two ends of the TCA on the body with Sil-Poxy Silicone Adhesive (Smooth-On
57 Inc.).
58
59

60 Reshape the body. The reason to reshape the body is to circumvent difficulties in direct
61 fabricating a soft body that has channels in a complex shape. For example, we use pre-stretching
62 to create a curved shape for the gripper and thus a curved U shape for the TCA, which is very
63
64

1 difficult to create using the conventional molding method. For the twisting manipulator, we use
2 a wrapping method to arrange a TCA into a helical shape.
3
4

5 Assemble bodies together. If there are multiple bodies that are actuated separately by TCAs,
6 we can assemble them together. For example, the soft robotic arm is an assembly of the three in-
7 dividual modules. Sometimes, assembling and reshaping happen at the same time, for example,
8 wrapping a TCA on a cylinder in a helical shape.
9
10
11
12
13
14
15
16
17
18

19 **9 The fabrication process of the 2D bending module: gripper**

20
21
22
23
24
25
26
27
28
29
30
31
32
33
34
35
36
37
38
39
40
41

42 We first fabricate a soft body with channels as shown in Fig. 7. Then we use a force stand
43 (MARK-10, ESM 303) to drag a layer of a silicone tape (LOCTITE, Go2) 120%, and stick
44 another layer of the silicone tape that is not stretched on it. After that we sew a TCA (87 mm)
45 into the channels of the soft body as a U shape, make electrical leads and fix the two ends of
46 the TCA on the soft body. The body is bonded to the tape that is not stretched using Sil-Poxy
47 Silicone Adhesive. After the adhesive cures (2 hours), we release the stretching and the whole
48 assembly becomes a curved shape.
49
50
51
52
53
54
55
56
57
58
59
60

42 **10 The fabrication process of the twisting module**

43
44
45
46
47
48
49
50
51
52
53
54
55
56
57
58
59
60

42 We first fabricate a soft cylindrical body (diameter 6 mm, length 18 mm) and a soft tube
43 (inner diameter 0.9 mm and outer diameter 2.5 mm) with Ecoflex 30. Then we sew a TCA (140
44 mm) into the tube to make a TCA-tube assembly. After that, we make two leads and fix the
45 two ends of the TCA on the tube. The soft cylindrical body has a channel at its center allows
46 electrical wires running through it.
47
48
49
50
51
52
53
54
55
56
57
58
59
60

42 For the single-helix twisting module, we directly wrap the TCA-tube assembly on the cylin-
43 drical body. For the double-helix twisting module, we first fold the TCA-tube assembly and
44
45
46
47
48
49
50
51
52
53
54
55
56
57
58
59
60

1
2 then wrap it on the cylindrical body. After that, we fix the two ends of the TCA-tube assembly
3
4 on the body with Sil-Poxy Silicone Adhesive.
5
6
7
8

9 **11 The fabrication process of the 3D bending module**

10
11
12

13 We first fabricate a soft body with 3 parallel channels along its perimeter (an additional
14 channel at its center allows electrical wires running through it), sew 3 TCAs (45 mm for each)
15 of the same length into the channels in three directions. Then we make two leads on each TCA
16 and fix the ends of the TCAs on the body. After that, we fixed the manipulator on a 3D printed
17 solid base.
18
19
20
21
22
23
24
25
26
27

28 **12 Experiments for characterization of the 2D bending module: gripper**

29
30
31
32
33

34 To obtain the relationship between the opening width and the input power, we first calculate
35 the required current corresponding to a specific power by measure the resistance of the TCA
36 (assume the resistance is constant). A DC regulated power supply (Tekpowe, TP 3005T) is
37 used to supply the required current. We record a video of the opening process for 2 s when a
38 current is applied. Tracker software (<https://physlets.org/tracker/>) is used to process the videos
39 and extract the opening width.
40
41
42
43
44
45
46
47

48 To find the relationship between the gripping force and the opening width, we use a force
49 stand (MARK-10, ESM303 with M5-2 Force gauge) to drag the two ends of the gripper using
50 two strings. The force stand is equipped with an encoder, so that it allows us to export the
51 opening width and the force simultaneously. The experiments are repeated 3 times.
52
53
54
55
56
57
58
59
60

1 2 **13 Experiments for characterization of the twisting module** 3 4

5 First, the module is bond to a rigid base, and a carbon fiber rod is stuck to the top of the
6 manipulator, and the power supply (Tekpowe, TP 3005T) is used to supply the required current
7 corresponding to a specific power. The rotation processes are recorded and the rotational angle
8 is extracted using Tracker software.
9
10
11
12
13

14 **Experiments for characterization of the 3D bending module** 15 16

17 We place two markers on the end of the module and the top of the rigid base, respectively,
18 as shown in Fig. s8. Marker 1 is used to calculate the origin of the module's frame, which is the
19 connection point of the module and the rigid base (Marked as O). Marker 2 is stuck at the end
20 of the module. The radius of the marker is 3 mm and the weight is 0.24 g.
21
22
23
24
25
26
27
28
29
30
31
32

33 **15 Fabrication and Control of the soft robotic arm** 34 35

36 The gripper, the twisting module and the 3D bending module are connected in serial using
37 Sil-Poxy Silicone Adhesive. All the common ground wires are connected together as one to
38 reduce the number of wires.
39
40
41
42
43

44 We use five motor drivers (MC33926 Motor Driver Carrier) to apply electricity to five TCAs
45 in the manipulators (1 in the gripper, 1 in the twisting module and 3 in the 3D bending module).
46
47 An Arduino board is used to control the motor drivers.
48
49
50
51
52
53

54 **16 Supplementary Videos** 55 56

- 57 1. s1 Overcome Friction.mp4
58
59 2. s2 Overcome Gravity.mp4
60

1
2 3. s3 Gripper Characterization.mp4
3
4
5 4. s4 Twisting Module.mp4
6
7
8 5. s5 3D bending Module.mp4
9
10
11 6. s6 Soft Robotic Arm.mp4
12
13
14
15
16
17
18
19
20
21
22
23
24
25
26
27
28
29
30
31
32
33
34
35
36
37
38
39
40
41
42
43
44
45
46
47
48
49
50
51
52
53
54
55
56
57
58
59
60

For Peer Review

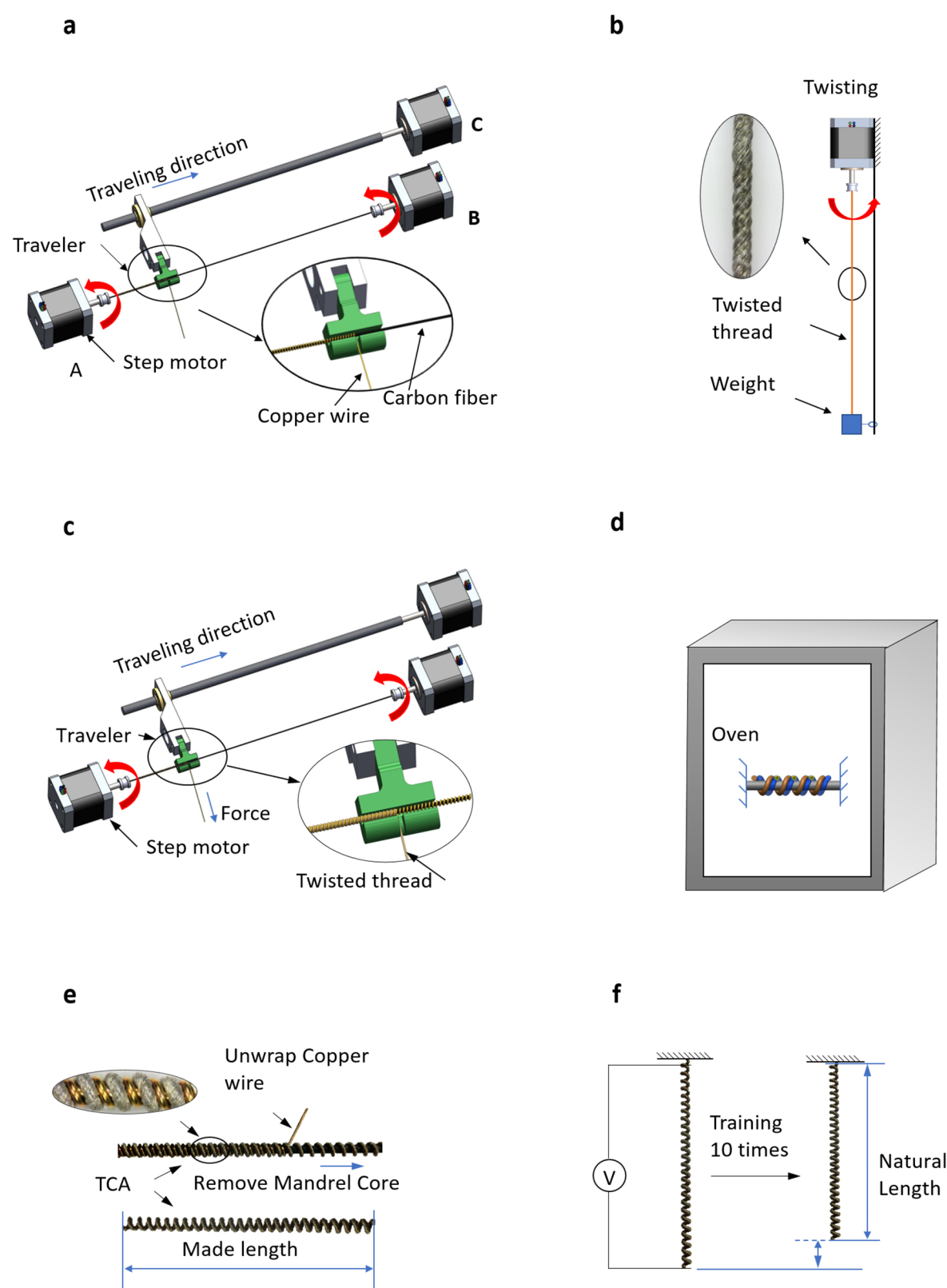


Fig. s 1. The fabrication process of TCAs with free strokes. (a) Make the helical mandrel on the machine. (b) Twist a thread. (c) Coil the twisted thread in the groove on the helical mandrel using the machine. (d) Anneal the TCA with the mandrel. (e) Remove the TCA from the mandrel. (f) Train the TCA to get a reversible free stroke.

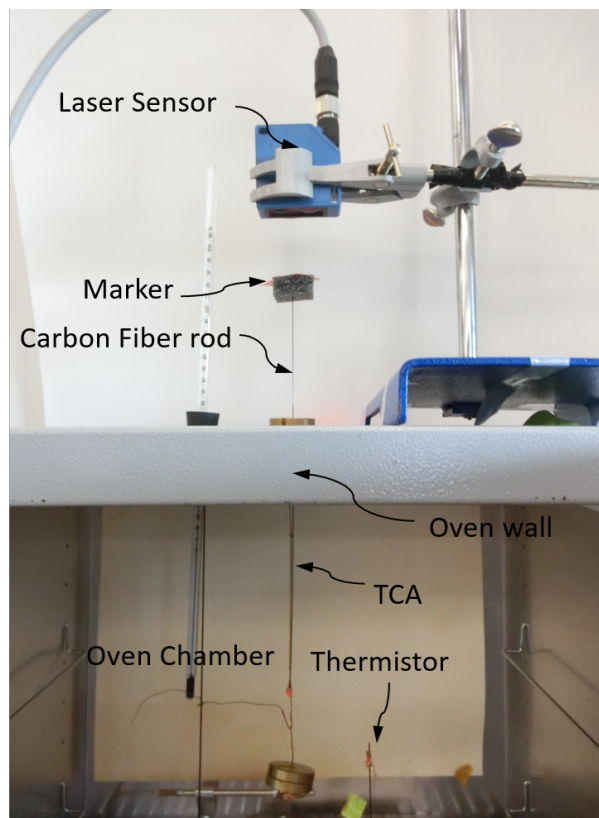


Fig. s 2. The experimental setup to obtain the displacement-temperature relationship in the oven. Note that only a small part of the oven is shown in this figure.

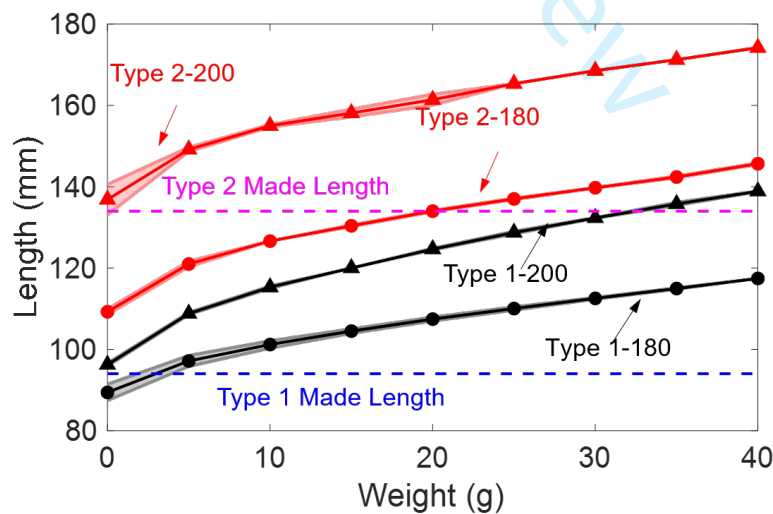


Fig. s 3. The steady-state length of the two types of TCAs corresponding to different weights after the creeping process.

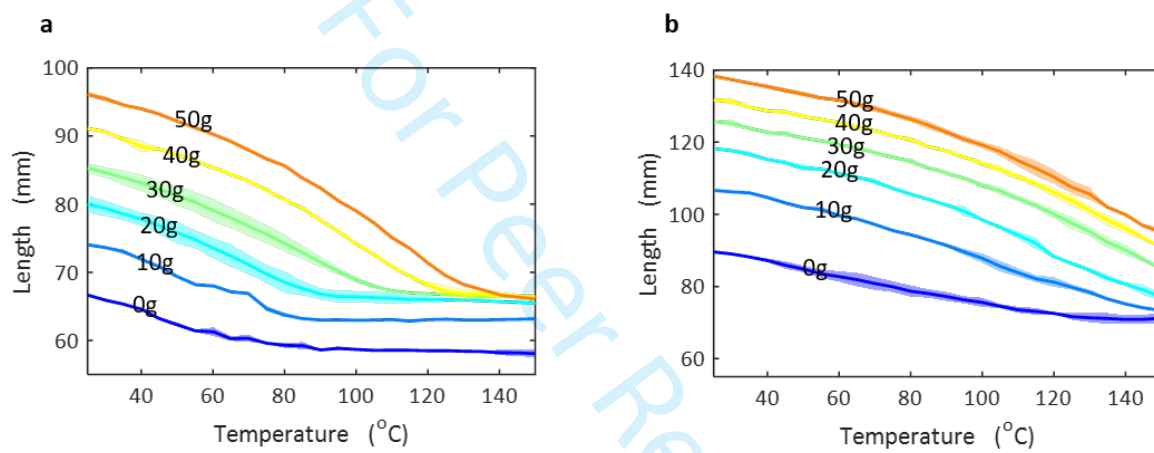


Fig. s 4. The experimental results of a TCA with free strokes. Length with respect to temperature. Solid lines indicate the average and shaded regions indicate the standard deviation. (a) and (b) are corresponding to the Fig. 4 b and c in the main text.

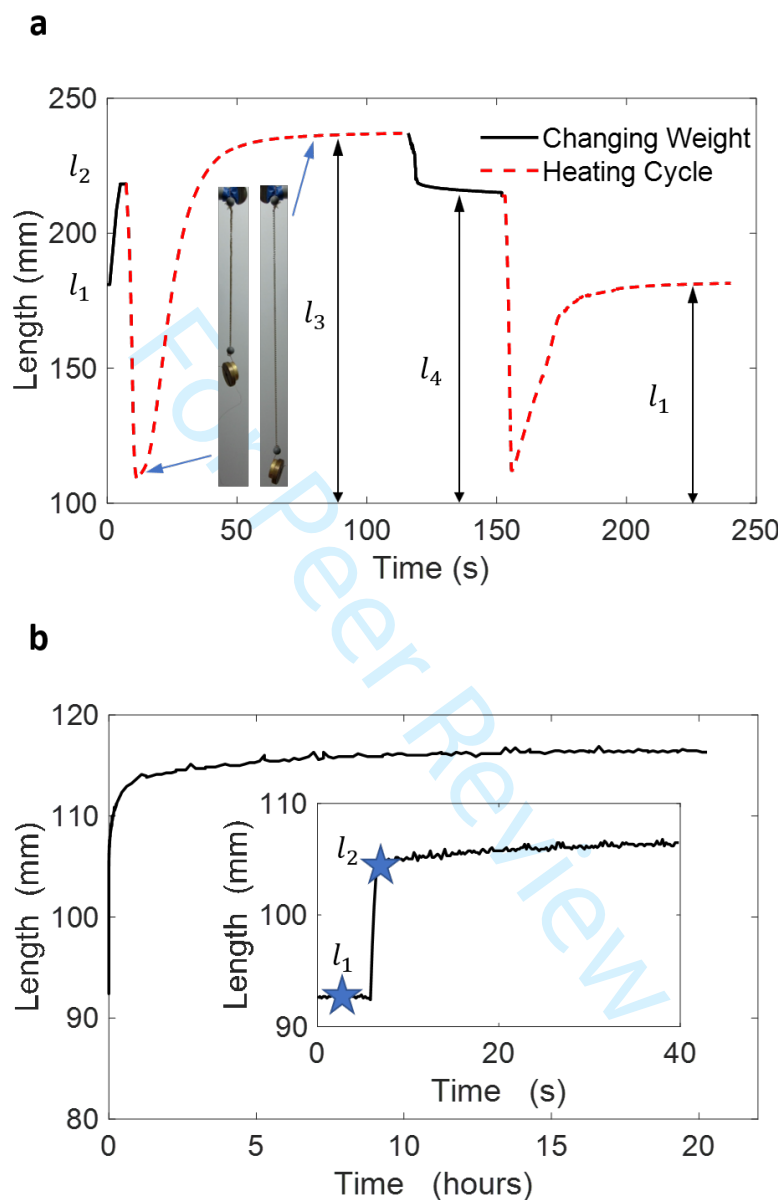


Fig. s 5. Temporary length (a) An experiment demonstrating the temporary length with a weight hanging at a TCA's end. (b) A creeping process that lasts for 20 hours.)

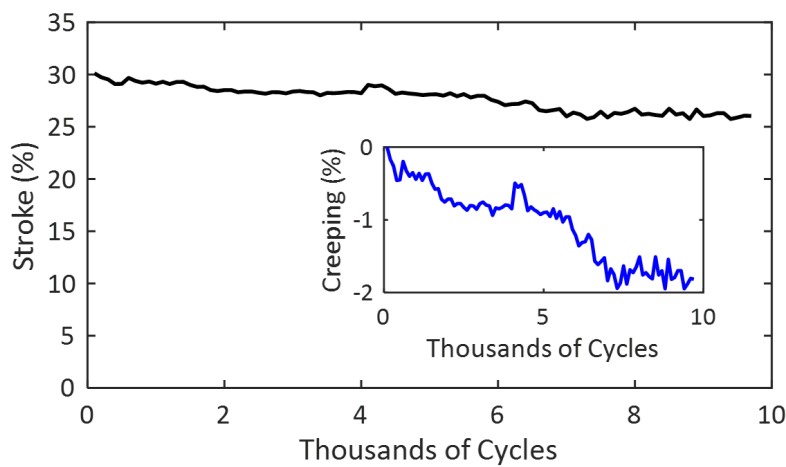


Fig. s 6. Tensile stroke versus actuation cycle for a Type 1-180 TCA that is driven electrothermally at 0.25 Hz under a 2-MPa load (each point averages 100 cycles). The inset provides creep (decrease of the stroke) as a function of cycle.

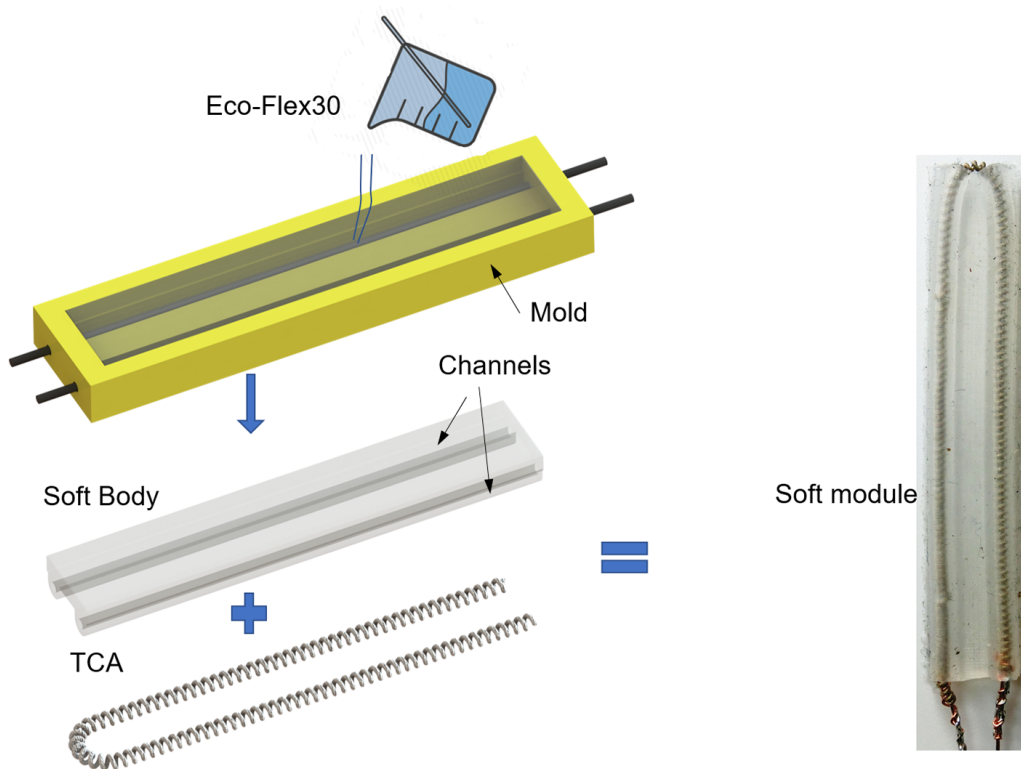


Fig. s 7. The fabrication process of the soft modules with an example.

1
2
3
4
5
Jiefeng Sun
6
7
8
9
10

Reference for Response Letter

- [1]. Sun J, Pawlowski B, Zhao J. Embedded and controllable shape morphing with twisted-and-coiled actuators. In: 2018 IEEE/RSJ International Conference on Intelligent Robots and Systems (IROS); 2018.(pp. 5912-7). IEEE.
- [2]. Zhang J, Simeonov A, Yip M C. Three-dimensional hysteresis compensation enhances accuracy of robotic artificial muscles. Smart Materials and Structures 2018;27:035002.
- [3]. Konda R, Zhang J. The Effects of Nylon Polymer Threads on Strain-Loading Hysteresis Behavior of Supercoiled Polymer (SCP) Artificial Muscles. In: ASME 2019 Dynamic Systems and Control Conference. American Society of Mechanical Engineers Digital Collection.
- [4]. Haines C S, Lima M D, Li N, *et al.* Artificial muscles from fishing line and sewing thread. science 2014;343:868-72.
- [5]. Aziz S, Naficy S, Foroughi J, *et al.* Characterisation of torsional actuation in highly twisted yarns and fibres. Polymer testing 2015;46:88-97.
- [6]. Piao C, Jang H, Lim T, *et al.* Enhanced dynamic performance of twisted and coiled soft actuators using graphene coating. Composites Part B: Engineering 2019;178:107499.
- [7]. Wu L, Tadesse Y. Modeling of the electrical resistance of TCP muscle. In: ASME 2017 International Mechanical Engineering Congress and Exposition; 2017. American Society of Mechanical Engineers Digital Collection.
- 11
12
13
14
15
16
17
18
19
20
21
22
23
24
25
26
27
28
29
30
31
32
33
34
35
36
37
38
39
40
41
42
43
44
45
46
47
48
49
50
51
52
53
54
55
56
57
58
59
60